TU Delft Delft University of Technology

MASTER THESIS

INHIBITION MECHANISMS OF ORGANIC COMPOUNDS ON COPPER AND COPPER ALLOYS

Student:	Bingyu Li (4479602)
Program of Study:	M.Sc. Materials Science and Engineering (MSE)
Specialization:	Metals Science and Technology
Supervisors:	Dr. J.M.C. Mol
	Dr. P. Taheri
Graduation Date:	2017/07/05

The faculty of Mechanical, Maritime and Materials

Engineering (3mE)

Inhibition mechanisms of organic compounds on copper and copper alloys

Master thesis

Bingyu Li

Supervisors： Dr. J.M.C. Mol

Dr. P. Taheri

ABSTRACT

Because of a series of predominant properties, copper and copper alloys are used nowadays in the production and manufacturing industries. Amongst all available copper alloys, brass, with a relative low cost, is one of the most common materials with a wide range of applications, such as heat exchangers and maritime industry. Corrosion is a common phenomenon for copper and brass in their various applications resulting in serious consequences and direct as well as indirect economic losses. Therefore, a high degree of attention should be paid to their corrosion control. The usage of corrosion inhibitors is one of the efficient approaches to retard corrosion of copper and brass.

This master thesis focused on three organic corrosion inhibitors, i.e. imidazole, 2-mercapto-benzimidazole (MBI) and 2-mercapto-1-methyl-benzimidazole (1H-HB-2T). Open Circuit Potential (OCP) measurement, Linear Polarization Resistance (LPR) measurement and Electrochemical Impedance Spectroscopy (EIS) were used together with Fourier Transform Infrared Spectroscopy (FTIR, both ex-situ FTIR and in-situ FTIR) to evaluate their inhibition efficiencies and interaction mechanisms, where the latter inhibitors were studied in more details.

The results collected in this master thesis show the following: (1) different organic inhibitors provided different inhibition effects on copper and brass; (2) One kind of inhibitor had different inhibition effects on copper and brass; (3) the inhibition effects of MBI and 1H-HB-2T on copper and brass were linked with an electrostatic interaction between their molecules and the surface of specimens; (4) during the physisorption process at the specimen/solution interface, interfacial bonds were formed and a thin but protective layer was produced on the surface of immersed specimens, but these interfacial bonds could break because of soluble aggressive species in the environment resulting in a diminished corrosion protection; (5) the time required for the interfacial bond to break depends on the inhibitor and specimen types.

CONTENTS

PART Ⅰ SCIENTIFIC ARTIFIC ..... **i**

PART Ⅱ THESIS REPORT ..... **ix**

LIST OF FIGURES x

CHAPTER 1 INTRODUCTION 1

1.1 Copper and copper alloys 1

1.2 Corrosion and corrosion protection 3

1.3 Corrosion inhibitor 4

1.4 Aims of this master thesis 6

Chapter 2 EXPERIMENTS and MATERIALS 7

2.1 Open Circuit Potential measurement 7

2.1.1 Introduction of OCP measurement 7

2.1.2 Experimental procedure of OCP measurement 8

2.2 Linear Polarization Resistance measurement 9

2.2.1 Introduction of LPR measurement 9

2.2.2 Experimental procedure of LPR measurement 10

2.3 Electrochemical Impedance Spectroscopy 11

2.3.1 Introduction of EIS 11

2.3.2 Experimental procedure of EIS 13

2.4 Fourier Transform Infrared Spectroscopy 14

2.4.1 Introduction of FTIR spectroscopy 14

2.4.2 Experimental procedure of FTIR spectroscopy 14

2.5 Specimens 15

2.5.1 Specimens for inhibitors pre-selection 15

2.5.2 Specimens for detailed analysis of inhibitors 17

2.5.3 Cleanness of equipments 20

2.6 Inhibitors 21

2.6.1 Imidazole 21
2.6.2 2-mercapto-benzimidazole 22
2.6.3 2-mercapto-1-methyl-benzimidazole 22

Chapter 3 RESULTS and DISCUSSIONS 23
3. 1 Pre-selection of inhibitors 23
3.2 Investigation on the inhibition mechanisms 28
3.2.1 Investigation on the adsorption 28
3.2.1.1 Adsorption of 1 mmol/100ml MBI 29
3.2.1.2 Adsorption of 1 mmol/100ml 1H-HB-2T 30
3.2.2 Investigation on the interfacial interactions 30
3.2.2.1 1 mmol/100ml MBI on pure copper thin film 31
3.2.2.2 1 mmol/100ml MBI on 50% Zn copper alloy thin film 34
3.2.2.3 1 mmol/100ml MBI on pure zinc thin film 36
3.2.2.4 1 mmol/100ml 1H-HB-2T on pure copper thin film 39
3.2.2.5 1 mmol/100ml 1H-HB-2T on 50% Zn copper alloy thin film 42
3.2.2.6 1 mmol/100ml 1H-HB-2T on pure zinc thin film 45

Chapter 4 CONCLUSIONS 49

APPENDIX A I
APPENDIX B II
APPENDIX C IV
APPENDIX D VI
APPENDIX E VIII
APPENDIX F X
APPENDIX G XII
REFERENCES XIV
ACKNOWLEDGEMENTS XVII

Master Thesis

TU Delft Delft University of Technology

Inhibition mechanisms of organic compounds on copper and copper alloys

Part I:
SCIENTIFIC ARTICLE

Inhibition mechanisms of organic compounds on copper and copper alloys

Abstract

Copper and brass are used widely in different industries, but corrosion results in serious failures limiting their applications. The usage of corrosion inhibitors is an efficient approach to control or prevent corrosion of copper and brass in some specific applications, such as heat exchangers. Since the inhibition effects of 1 mmol/100ml 2-mercapto-benzimidazole (MBI) and 2-mercapto-1-methyl-benzimidazole (1H-HB-2T) on copper and brass were similar, this scientific article mainly focused on imidazole and MBI. By means of electrochemical and FTIR measurements, imidazole was proved to exhibit weaker interfacial bonds than those of MBI, while MBI only worked well on copper and brass and not on zinc. The inhibition mechanism of MBI was linked with physisorption promoted by electrostatic interaction.

Keywords: Copper, Brass, imidazole, MBI, Inhibition mechanisms

1. Introduction

Copper and copper alloys are ancient materials with a long history in human society. Because of their attractive combination of mechanical, thermal and electrical properties, they serve human in a wide region. Amongst all copper alloys, brass, with a relative low cost, is commonly used for heat exchangers and water pipelines.

Zinc, as a principal alloying element of brass, is significant for enhancing its mechanical properties and corrosion resistance[1]. The good anti-corrosion ability of brass is mainly related to a stable and protective passivation film composed of copper and zinc oxide [2]. However, this film is not fully protective in certain circumstances. For example, brass can suffer preferential dissolution of zinc when it is exposed to the electrolyte with Cl^- or Br^- ions[3]. Therefore, although brass has good corrosion resistance, corrosion in certain situations still cannot be ignored.

At present, corrosion inhibitors are used to mitigate or prevent corrosion of copper and brass in certain applications. According to ISO, a corrosion inhibitor is defined as a chemical substance that can decrease the corrosion rate when it is present in a specific corrosion system at a suitable concentration, without changing the concentration of any other corrosion agent significantly[4]. Its protection mechanism is mainly related to interactions at the specimen/solution interface, during which interfacial bonds are formed and produce a productive mono-layer on the surface. Organic corrosion inhibitors are attractive in various corrosive media[5]. As Fouda stated that their corrosion inhibitions are mainly related to their capacity to be adsorbed on the specimen[6]. Here, two types of adsorption, physisorption (by electrostatic force) and chemisorption (by charge sharing or charge transfer), are mainly considered[7].

The main aim of this article was investigating inhibition behaviors and inhibition mechanisms of 1 mmol/100ml imidazole and MBI on copper and brass.

2. Experiments and Materials

2.1 Research approach

This thesis was divided into two parts with different purposes. In the first stage, Linear Polarization Resistance (LPR) measurement was employed for inhibitors screening by comparing the polarization resistances of specimens. Then, the one with better inhibition effect was chosen for the second stage of analysis on its inhibition mechanism by means of Electrochemical Impedance Spectroscopy (EIS) and Fourier Transform Infrared Spectroscopy (FTIR).

2.1.1 LPR measurement

LPR measurement is a widely used method to obtain the corrosion rate and the polarization resistance directly. The polarization resistance Rp is defined as the difference of real impedances at lower and higher frequency. Combining the equation 2.1 and the fact that corrosion rate is proportional to corrosion current density i_{corr}, Rp is inversely proportional to corrosion rate.

$$R_p = \frac{\beta_a \beta_c}{2.3 \times i_{corr}(\beta_a + \beta_c)} \qquad \text{eq. 2.1}$$

where β_a and β_c are the anodic and cathodic Tafel constants.

2.1.2 EIS

EIS was employed to investigate corrosion kinetics and the corrosion protection mechanism of an organic inhibitor. Direct information of the corrosion system was represented in Nyquist plot and Bode plot, while its detailed physical meanings were provided by an equivalent circuit with different elements[8]. Priority attentions in EIS was setting up a fit and meaningful equivalent circuit to explain the electrochemical failure at the specimen/coating interface[9].

2.1.3 FTIR Spectroscopy

Since absorption only happens when the frequency of the incident light is equal to the vibration frequency of a bond and the vibration frequency is a characteristic of a specific molecule, FTIR spectroscopy can collect an infrared spectrum of the absorption behavior of organic inhibitors and provide information of their vibration states. Both ex-situ and in-situ FTIR spectroscopy were used in this thesis to study the interaction mechanisms of an organic inhibitor, the former one explained its absorption type, while the later one described its interfacial interaction with specimens (formation or break of interfacial bonds).

2.2 Specimens

Because of the Kretschmann geometry of in-situ FTIR spectroscopy, specimens used in two stages for different purposes were different. Zinc was included in both stages since it was a principal alloying element of brass.

2.2.1 Specimens for inhibitors screening

Copper, 10% Zn copper alloy, 30% Zn copper alloy, 40% Zn copper alloy and zinc were studied for pre-selection of inhibitors. Copper and zinc were 30 mm×30 mm flat sheets, while brass were cylindrical with 1 mm thickness

and 11 mm diameter. They were polished mechanically with silicon carbide paper (from 320 to 4000).

2.2.2 Specimens for detailed analysis

Because of the limited penetration depth of incident light and the Kretschmann geometry of in-situ FTIR spectroscopy shown in the figure 2.2, the specimen and internal reflection element (IRE) were required to contact closely. This direct contact was carried out by physical vapor deposition (PVD). As a widely used vacuum deposition method, PVD can produce metal vapor and deposit a nano-scale metal film on IRE easily. But different metals have different melting temperatures, so it is difficult to control the composition ratio of an alloy film. Therefore, only copper, 50% Zn copper alloy (with a rough volume ratio 1:1) and zinc thin film with 13.3 nm thickness were used for detailed analysis of the chosen inhibitor on its interaction mechanism.

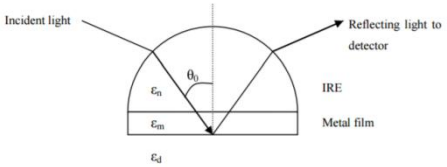

Figure 2.2 The Kretschmann geometry

2.3 Corrosion inhibitors

In this article, imidazole and MBI were compared and studied on their corrosion inhibitions and mechanisms on copper and brass. Their structures are shown in the figure 2.3. Their concentration in 3 wt% NaCl solution was 1mmol/100ml.

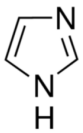

(a)

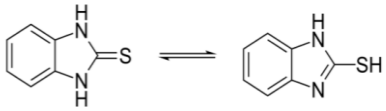

(b)

Figure 2.3 The structure of (a) imidazole, (b) MBI

3. Results and Discussions

3.1 Inhibitors screening

Initially, the polarization resistances of specimens in 1 mmol/100ml imidazole and MBI were compared. It is shown in the figure 3.1, from which imidazole was proved to own a worse effect on copper and brass based on its lower polarization resistance. Hence, MBI was chosen for the following analysis on its interaction mechanism on copper and brass.

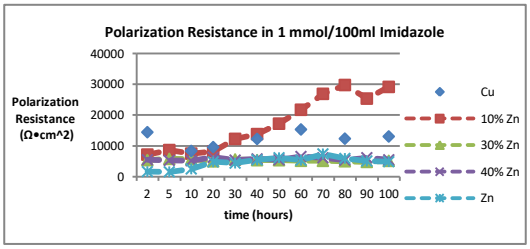

(a)

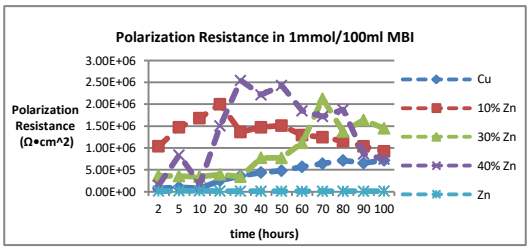

(b)

Figure 3.1 Polarization resistances of specimens in 1 mmol/100ml (a) imidazole, (b) MBI

3.2 Investigation on the interaction mechanisms

3.2.1 Investigation on the adsorption

Ex-situ FTIR spectroscopy was employed to explain the adsorption type

of MBI on specimens. The ex-situ FTIR spectrum of 1 mmol/100ml MBI is shown in the figure 3.2. MBI functional groups mainly produced peaks in the wavenumber range from 900 to 1550 cm^{-1}[10-11]. A broad peak also appeared in this range for specimens which had exposed to MBI for 30 min. This broad peak was caused by an overlap of various peaks, so the existence of various MBI functional groups on the surface of specimens could be proved. Namely, the whole MBI molecule was adsorbed on specimens by electrostatic force.

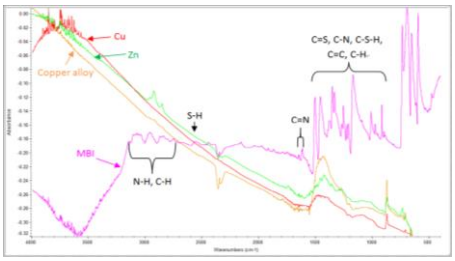

Figure 3.2 The ex-situ FTIR spectrum of MBI

3.2.2 Investigation on the interfacial interactions

In-situ FTIR spectroscopy was used to collect quantitative and qualitative information on the interfacial interactions between specimens and inhibitors (formation or degradation of interfacial bonds). Since the peak intensity of liquid water kept unchanged during immersion, the relative peak intensities of various functional groups ($\frac{\text{peak intensity of a functional group}}{\text{peak intensity of liquid water}}$) and its changes in 30 hours were important.

3.2.2.1 MBI on pure copper

MBI functional groups are possibly C-N, C=N, C-S and S-H (or C-S-H), C=S, C=C and C-H in aromatic, their wavenumbers and changes of relative peak intensities in 30 hours are shown in the figure 3.3. The relative peak intensities of peaks produced by MBI functional groups rose to the maximum after 5 hours, so MBI functional groups appeared on the copper surface increased in the first 2 to 10 hours and decreased afterwards. It meant that after 2 to 10 hours, interfacial bonds between MBI molecules and copper surface broke resulting in diminished inhibition of MBI.

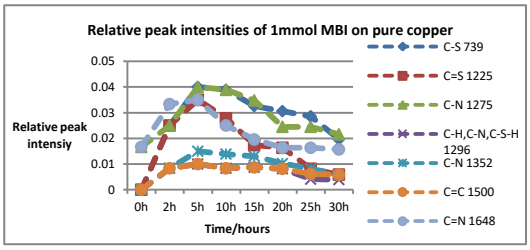

Figure 3.3 The relative peak intensities of MBI functional groups on copper

Similar information was also collected from EIS. Nyquist plot and Bode plot are shown in the figure 3.4. In Nyquist plot, the radius of the semi-circle increased initially and arrived at its maximum value after 5 hours. Then, it reduced. Since the impedance at high frequency (left of the X-axis) was equal to the ohmic resistance which kept constant, while that at low frequency (right of the X-axis) was equal to the sum of the polarization resistance and the ohmic resistance, the increasing radius in the first 2 to 10 hours reflected the increasing polarization resistance of copper immersed in the 1 mmol/100ml MBI solution, which resulted in a strengthened anti-corrosion ability. Afterwards, the corrosion resistance of copper began to decrease. Although similar trend was not clear in Bode plot, it was convincing proved by an equivalent circuit and corresponding

impedance data attached in the Appendix B.

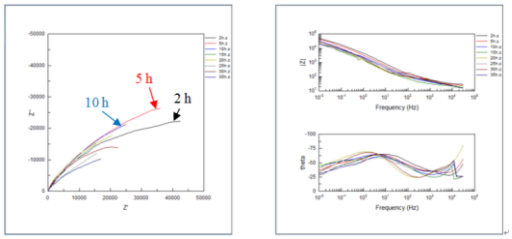

Figure 3.4 Nyquist (left) plot and Bode (right) plot of MBI on copper

In the detailed polarization resistance trend of copper shown in the figure 3.5, a peak appeared after 7 hours. It fit what got from EIS. Combined with results of in-situ FTIR spectroscopy, it is rational to conclude that 1 mmol/100ml MBI could provide protection against corrosion on copper for 2 to 10 hours, then, its corrosion protection became weak because of the break of interfacial bonds.

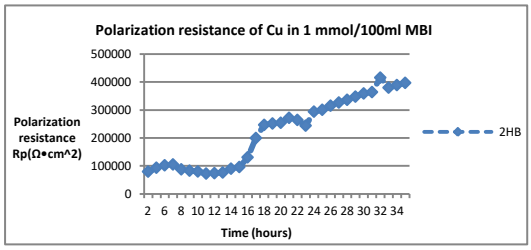

Figure 3.5 Polarization resistance of copper in MBI

3.2.2.2 MBI on 50% Zn copper alloy

The information of MBI functional groups is shown in the figure 3.6. From the figure 3.6, MBI functional groups appeared on the brass surface increased in the first 15 hours, then, a decrease happen. Hence, the break of interfacial bonds between the alloy surface and MBI molecules happened after 10 to 20 hours of immersion resulting in its weakened inhibition effect.

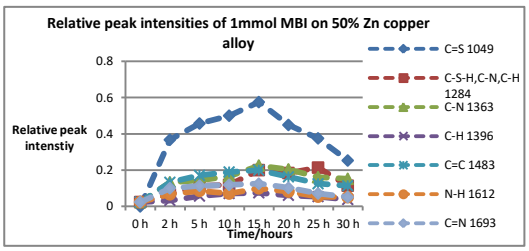

Figure 3.6 The relative peak intensities of MBI functional groups on 50% Zn copper alloy

Nyquist plot and Bode plot are shown in the figure 3.7. Since curves in Bode plot were too dense, more attention was paid to Nyquist plot. According to Nyquist plot, the polarization resistance of 50% Zn copper alloy increased and arrived at its maximum value when the immersion time was 15 hours. This trend showed that the strengthened anti-corrosion ability of the alloy would become weak after 10 to 20 hours. It could be further proved by an equivalent circuit attached in the Appendix C.

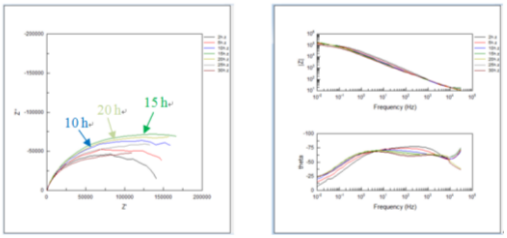

Figure 3.7 Nyquist (left) plot and Bode (right) plot of MBI on 50% Zn copper alloy

Overall, a conclusion can be made that 1 mmol/100ml MBI could provide corrosion protection on 50% Zn copper alloy. But its effect weakened after 10 to 20 hours because of the break of interfacial bonds with the brass surface.

3.2.2.3 MBI on pure zinc

The figure 3.8 expresses the wavenumbers of MBI functional groups and the relative peak intensities changes of their peaks. In this figure, peaks

appeared after 2 and 15 hours were linked with the formation and re-formation of bonds at zinc/solution interface, while the decreases after peaks were related to the break of interfacial bonds. Namely, the best effect of 1 mmol/100ml MBI on zinc appeared when the immersion time was within 5 hours and between 10 and 20 hours.

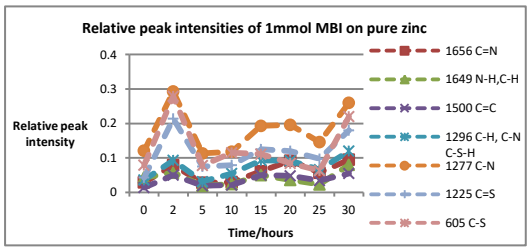

Figure 3.8 The relative peak intensities of MBI functional groups on zinc

Nyquist plot and Bode plot of 1 mmol/100ml MBI on zinc are shown in the figure 3.9. Since EIS was unstable in the early measuring time, information provided by curves measured after 2 hours was not persuasive. Besides, curves in Bode plot were dense, attention was mainly paid to Nyquist plot. According to Nyquist plot and the equivalent circuit attached in the Appendix D, the polarization resistance of zinc reached its peak after 15 hours. Therefore, the best corrosion resistance of zinc was verified to appear after 10 to 20 hours of exposure.

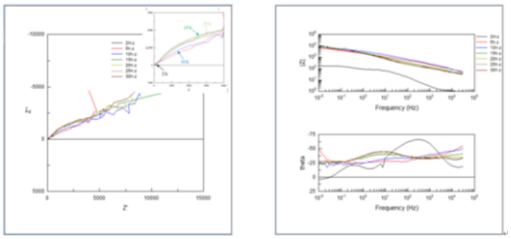

Figure 3.9 Nyquist (left) plot and Bode (right) plot of MBI on zinc

However, in the detailed trend of zinc polarization resistance plotted in the figure 3.10, different information was given (a peak appeared after 9 hours rather than 10 to 20 hours). One possible reason was linked with different surface conditions. In EIS and in-situ FTIR spectroscopy, deposited zinc film with mirror like surface was tested, while in LPR measurement, zinc sheet polished with sandpaper (from 320 to 4000) was tested. Another reason was the fact that different organic inhibitors might behave differently on different specimens. It could be certified by the figure 3.1 as well as studies of Zarrouk[12]. Although 1 mmol/100ml MBI behaved well on copper and brass, it might not reduce the corrosion rate of zinc dramatically although it could also be adsorbed on the zinc surface.

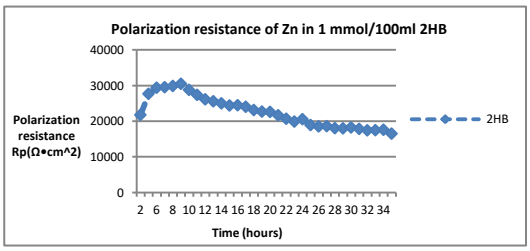

Figure 3.10 Polarization resistance of zinc in MBI

4. Conclusion

- Imidazole exhibits a weaker inhibition on copper and brass compared with MBI.
- MBI works well on copper and brass, but on zinc.
- The inhibition mechanism of MBI on copper and brass is linked with an electrostatic interaction with the specimens, during which interfacial bonds are formed at the specimen/solution interface to produce a protective layer.

- Aggressive species in the solution breaks interfacial bonds after few hours resulting in diminished inhibition of MBI.

References

[1]S.Hosseinpour, M.Forslund, C.M. Johnson, et al. "Atmospheric corrosion of Cu, Zn and Cu-Zn alloys protected by self-assembled monolayers of alkanethiols", *Surface Science*, Vol.648, 2016, pp. 170-176

[2] M.B.Radovanovic, M.M.Antonijevic. "Inhibition of brass corrosion by 2-Mercapto-1-methylimidazole in weakly alkaline solution", *Journal of Materials Engineering and Performance*, Vol.25, Issue 3, 2016, pp.921-937

[3]H.Fan, S.Li, Z.Zhao, et al. "Inhibition of brass corrosion in sodium chloride solutions by self-assembled silane films", *Corrosion Science*, Vol.53, Issue 12, 2011, pp.4273-4281

[4]T.A.Soylev, M.G.Richardson. "Corrosion inhibitors for steel in concrete: State-of-the-art report", *Construction and Building Materials*, Vol.22, Issue 4, 2008, pp.609-622

[5]B.Hmmouti, A.Dafali, R.Touzani, et al. "Inhibition of copper corrosion by bipyrazole compound in aerated 3% NaCl", *Journal of Saudi Chemical Society*, Vol.16, Issue 4, 2012, pp.413-418

[6]A.S.Fouda, S.M.Rashwan, M.Kamel, et al. "Unused meropenem drug as corrosion inhibitor for copper in acidic medium: experimental and theoretical studies", *International Journal of Electrochemical Science*, Vol.11, 2016, pp.9745-9761

[7]J.Aljourani, K.Raeissi, M.A.Golozar. "Benzimidazole and its derivatives as corrosion inhibitors for mild steel in 1 M HCl solution", *Corrosion Science*, Vol.51, Issue 8, 2009, pp.1836-1843

[8]G.Bierwagen, D.Tallman, J.Li, et al. "EIS studies of coated metals in accelerated exposure", *Progress in Organic Coatings*, Vol.46, Issue 2, 2003, pp.148-157

[9]http://www.metrohm-autolab.com/download/Applicationnotes/Autolab_Application_Note_EIS03.pdf

[10]M.R.Ahamed, S.F.Narren and A.S.Sadiq. "Synthesis of 2-mercaptobenzimidazole and some of its derivatives", *Journal of Al-Nahrain University*, Vol.16, Issue 2, 2013, pp.77-83

[11]M.G.Hosseini, T.Shanrabi and R.J.Nichols. "Characterization of mercaptobenzimidazole adsorption on an Au(111) electrode", *Iranian Journal of Science and Technology*, Transaction A, Vol.29, Issue A1, 2005, pp.49-63

[12]A.Zarrouk, B.Hammouti, A.Dafali, et al. "A theoretical study on the inhibition efficiencies of some quinoxalines as corrosion inhibitors of copper in nitric acid", *Journal of Saudi Chemical Society*, Vol.18, Issue 5, 2014, pp.450-455

Master Thesis

TU Delft Delft University of Technology

Inhibition mechanisms of organic compounds on copper and copper alloys

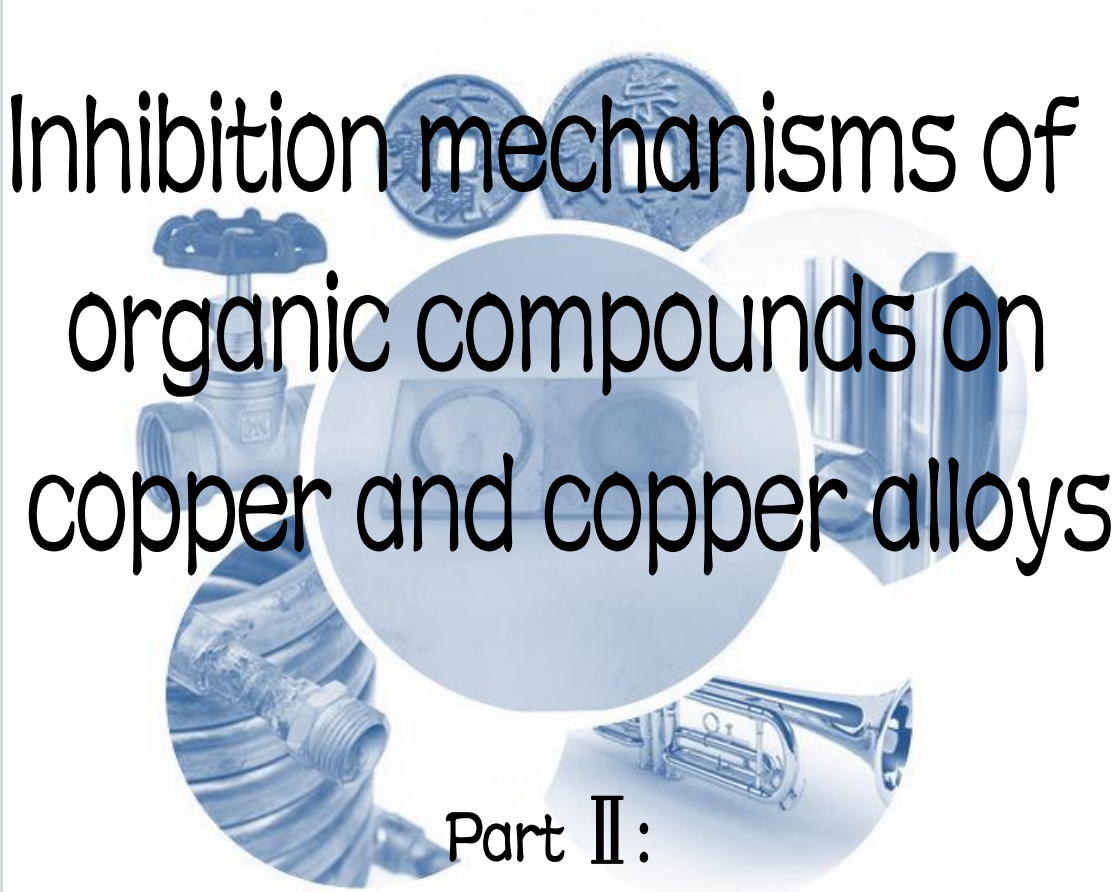

Part Ⅱ:
THESIS REPORT

LIST OF FIGURES

Figure 1.1 The Pourbaix diagram of copper 5

Figure 2.1 Working schematic diagram of a three-electrode corrosion cell 8

Figure 2.2 A simple equivalent circuit of corrosion 10

Figure 2.3 The schematic diagram of the calculation method of R_p 11

Figure 2.4 The schematic diagram of EIS 12

Figure 2.5 The current and voltage as a function of time 13

Figure 2.6 Nyquist plot and Bode plot 13

Figure 2.7 The microstructures of specimens for inhibitors pre-selection 16

Figure 2.8 The electrochemical system of OCP and LPR measurements 17

Figure 2.9 The Kretschmann geometry 18

Figure 2.10 The equipment (cell) for EIS and in-situ FTIR measurements 20

Figure 2.11 The electrochemical structure of EIS and FTIR measurements 20

Figure 2.12 The structure of imidazole 22

Figure 2.13 The structure of MBI 22

Figure 2.14 The structure of 1H-HB-2T 22

Figure 3.1 Polarization resistances of specimens immersed in 1 mmol/100ml inhibitors 24

Figure 3.2 Inhibition efficiencies of 1 mmol/100ml inhibitors 26

Figure 3.3 The ex-situ FTIR spectrum of 1 mmol/100ml MBI 29

Figure 3.4 The ex-situ FTIR spectrum of 1 mmol/100ml 1H-HB-2T 30

Figure 3.5 The baseline-corrected FTIR spectrum of 1 mmol/100ml MBI on pure copper thin film deposited on the Ge crystal in 30 hours 32

Figure 3.6 The relative peak intensities of MBI functional groups on pure copper thin film deposited on the Ge crystal in 30 hours 32

Figure 3.7 Nyquist (left) plot and Bode (right) plot of 1 mmol/100ml MBI on pure copper thin film deposited on the Ge crystal in 30 hours 33

Figure 3.8 Polarization resistance of copper in 1 mmol/100ml MBI in 35 hours 33

Figure 3.9 The baseline-corrected FTIR spectrum of 1 mmol/100ml MBI on 50% Zn copper alloy thin film deposited on the Ge crystal in 30 hours 35

Figure 3.10 The relative peak intensities of functional groups of MBI on 50% Zn copper alloy thin film deposited on the Ge crystal in 30 hours 35

Figure 3.11 Nyquist (left) plot and Bode (right) plot of 1 mmol/100ml MBI on 50% Zn copper alloy thin film deposited on the Ge crystal in 30 hours 36

Figure 3.12 The baseline-corrected FTIR spectrum of 1 mmol/100ml MBI on pure zinc film deposited on the Ge crystal in 30 hours 37

Figure 3.13 The relative peak intensities of functional groups of MBI on pure zinc film deposited on the Ge crystal in 30 hours 37

Figure 3.14 Nyquist (left) plot and Bode (right) plot of 1 mmol/100ml MBI on pure zinc thin film deposited on the Ge crystal in 30 hours 38

Figure 3.15 Polarization resistance of zinc in 1 mmol/100ml MBI in 35 hours 38

Figure 3.16 The baseline-corrected FTIR spectrum of 1 mmol/100ml 1H-HB-2T on pure copper film deposited on the Ge crystal in 30 hours 40

Figure 3.17 The relative peak intensities of functional groups of 1H-HB-2T on pure copper film deposited on the Ge crystal in 30 hours 41

Figure 3.18 Nyquist (left) plot and Bode (right) plot of 1 mmol/100ml 1H-HB-2T on pure copper thin film deposited on the Ge crystal in 30 hours 41

Figure 3.19 Polarization resistance of copper in 1 mmol/100ml 1H-HB-2T in 35 hours 42

Figure 3.20 The baseline-corrected FTIR spectrum of 1 mmol/100ml 1H-HB-2T on 50% Zn copper alloy film deposited on the Ge crystal in 30 hours 43

Figure 3.21 The relative peak intensities of functional groups of 1H-HB-2T on 50% Zn copper alloy film deposited on the Ge crystal in 30 hours 44

Figure 3.22 Nyquist (left) plot and Bode (right) plot of 1 mmol/100ml 1H-HB-2T on 50% Zn copper alloy thin film deposited on the Ge crystal in 30 hours 44

Figure 3.23 The baseline-corrected FTIR spectrum of 1 mmol/100ml 1H-HB-2T on pure zinc film deposited on the Ge crystal in 30 hours 46

Figure 3.24 The relative peak intensities of functional groups of 1H-HB-2T on pure zinc film deposited on the Ge crystal in 30 hours 46

Figure 3.25 Nyquist (left) plot and Bode (right) plot of 1 mmol/100ml 1H-HB-2T on pure zinc thin film deposited on the Ge crystal in 30 hours 47

Figure 3.26 Polarization resistance of zinc in 1 mmol/100ml 1H-HB-2T in 35 hours 48

CHAPTER 1 INTRODUCTION

1.1 Copper and copper alloys

Copper is one of the oldest metals used in human society, which firstly appeared in the prehistoric age civilization. Due to the attractive combination of mechanical, thermal and electrical properties, copper has been used in a wide range of applications in our daily life, such as artworks and fabricate structures. However, because of some restrictions on physical and chemical properties, its applications are limited in a certain range. Therefore, some new approaches are required to further extend the performances of copper in industrial and commercial applications. In order to fit these requirements, some alloying elements are added to produce various outstanding copper alloys, such as brasses (copper-zinc alloy), Aluminium bronzes (copper-aluminum alloy) and cupronickels (copper-nickel alloy). Compared with pure copper, those copper alloys with additional alloying elements have many enhanced properties. For example, they have a better machinability and formability, a higher thermal and electrical conduction and a better resistance to corrosion and biofouling. Hence, copper alloys can be extensively used to serve human in a wider range of environments and applications including heat conductors or heat exchangers in marine industry and saline water systems, water treatment units, and etc. At the same time, they are also more suitable in the electronic industry and the communication industry[1-2]. As stated by Boric that the demand of copper alloys in the world has outpaced all of its higher profile precious peers by a significant margin over the last 5 years [3]. Thus, detailed study on copper alloys is also valuable and significant for the further development of industries.

Amongst all available copper alloys, brass, with a relative low cost, is commonly used for marine industrial applications and esthetic purposes. Zinc, as a principal alloying element of brass, is pretty important not only for enhancing its mechanical properties including strength, wear resistance, machinability and hardness, but also for increasing its corrosion resistance in certain corrosive environments[4]. Overall, the superior properties of brass can be listed the following[5-6]:

(1) Relatively low melting point which varies from 900 to 940 ℃ depending on its composition;
(2) Relatively high density which varies from 8.4 to 8.73g/cm^3 depending on its composition;
(3) Either hard or soft depending on its composition;
(4) Higher malleability than either bronze (Cu-Sn) or zinc;
(5) Higher conductivity of heat and electricity;
(6) Desirable acoustic properties (appropriate for the use in musical instruments);
(7) Relatively low friction;
(8) Relatively high corrosion resistance, including galvanic corrosion in salt water;
(9) Not ferromagnetic;
(10) Almost 90% of brass can be recycled.

As mentioned above that brass can resist galvanic corrosion in certain aggressive media. Galvanic corrosion, is also called bimetallic corrosion, is an electrochemical process happened in an electrolytic liquid when two electrochemically different metals are closely and electrical contact. Combining with the fact that copper and zinc have different electrode potentials, it is easy to conclude that when copper-zinc alloy is immersed in an electrolyte, such as sodium chloride aqueous solution (NaCl solution), its corrosion rate is faster than that of pure copper or pure zinc because of the galvanic corrosion effect. However, the true situation is opposite. Generally, the main reason why brass has higher corrosion resistance than pure copper or pure zinc is believed to be related to the formation of a stable and protective thin film on its surface during the oxidation process. This passivation film is composed of copper and zinc oxide ($ZnO \cdot xH_2O$ and Cu_2O/CuO)[7].

However, this thin film is not fully protective in certain circumstances. For example, brass can suffer crevice corrosion and pitting corrosion when its surface is defective. Meantime, there is a trend for brass to undergo stress corrosion cracking when it is subjected to tensile stress in the corrosive environment. Furthermore, when brass is exposed to the electrolyte with Cl^- or Br^- ions, it can also suffer preferential dissolution of zinc from brass[8]. The phenomenon of preferential dissolution of zinc from brass is also termed as dezincification. Dezincification is one of the most common corrosion types of brass, especially in the industrial conditions. As reported that the degree of dezincification is linked with the zinc content in the brass, the higher the zinc content, the more serious of the negative effects caused by dezincification and the lower corrosion resistance of brass[9]. Overall, although brass has a higher corrosion resistance compared with pure copper and other copper alloys, corrosion happens in certain aggressive environments still cannot be ignored.

In this master thesis, copper and brass were main research materials for detailed investigation on their anti-corrosion ability in the 3wt% sodium chloride aqueous solution (NaCl solution).

1.2 Corrosion and corrosion protection

Corrosion, as a serious worldwide issue in the industry, is the degradation of pure metals or alloys caused by chemical or electrochemical reactions with the corrosive agents in the surrounding environment[10]. Amongst various types of corrosion in our daily life, aqueous metallic corrosion, in which the corrosive environment around the susceptive material is aqueous solution with soluble aggressive species, is most common. Generally, aqueous metallic corrosion can present in many different forms, such as corroded nails, leaking hot water tanks and reddish orange spots on car bodies.

Because of incorrect material choices, wrong processing choices, inappropriate surface treatment choices and etc., corrosion can happen easily. Hence, the surface of the susceptive metal or alloy becomes corroded and one or more kinds of stable compounds called corrosion products are produced on the material surface[11]. Costs for replacement of corroded equipments and work interruptions caused by damaged parts always occupy a relative irrational proportion in the national product of many industrialized countries. However, other than these direct consequences resulted from the corrosion phenomenon, there are some other indirect consequences which are more difficult to estimate and can also lead to some fateful issues. Overall, the harmful consequences of corrosion can be concluded the following[10]:

(1) Reduction of thickness which can lead to the reduction of material mechanical strength as well as the structural failure or breakdown;
(2) Reduction of surface properties which can lead to an increasing friction or a decreasing bearing ability;
(3) Change of physical properties of industrial or commercial equipments;
(4) Reduction of lifetime of industrial or commercial equipments or even plant shutdown;
(5) Reduction of working efficiency and goods value;
(6) Contamination of containing contents;
(7) Escape of containing contents and possible influence the surrounding environment;
(8) Mechanical damages caused by solid corrosion products;
(9) Added designing complexity or overdesign (e.g. thicker tube wall);
(10) Increasing investments of material, energy, water as well as human efforts.

Therefore, corrosion can lead to severe material loss as well as both direct and indirect economic loss. That is the reason why the importance of studies on corrosion control as well as corrosion prevention cannot be underestimated.

After years' investigations on corrosion phenomenon of different metals and alloys, various useful corrosion mitigation methods for protecting materials from corrosion in

aggressive environments have been discovered and they are listed the following:

(1) Correctly selection of materials and processing design;
(2) Protective coating, such as paints on the external surfaces;
(3) Sacrificial metals cathodic protection or impressed current cathodic protection;
(4) Adjusting the aggressive degree of the environment (e.g. change of pH value);
(5) Corrosion inhibitors

Amongst these practical approaches mentioned above, the usage of corrosion inhibitors plays a very significant role in certain applications, so the research subject of this master thesis was based on corrosion inhibitors.

1.3 Corrosion inhibitor

In order to distinguish corrosion inhibitors from other corrosion protection methods, such as protective coatings, International Organization for Standardization (ISO) defines that the corrosion inhibitor is a kind of chemical substance that can decrease the corrosion rate when it is present in a specific corrosion system at a suitable concentration, without changing the concentration of any other corrosion agent significantly[12]. The corrosion protection mechanism of a corrosion inhibitor is related to interfacial interactions between the inhibitor molecules and the metal or alloy surface, during which a protective mono-layer is formed in situ. Hence, the reaction rate of the anodic reaction (with an anodic inhibitor) or the cathodic reaction (with a cathodic inhibitor) or both of them (with a mixed inhibitor) can be reduced dramatically. Therefore, the corrosion process on the material surface can be controlled or even prevented.

During the corrosion process, an added anodic inhibitor can increase the anode potential, so a shift of the equilibrium from the corrosion zone in the Pourbaix diagram to the passivation zone happens. The Pourbaix diagram of copper is shown in the figure 1.1. Hence, a thin passivation oxide film can be formed at the anodic sites and reduces the effective anode area. In this way, the anodic reaction is slowed down and the oxidation reaction which happens in the anodic path is depressed resulting in the reduced corrosion rate, then, materials is protected against corrosion[13]. Similarly, an added cathodic inhibitor can reduce the rate of cathodic reaction, but the reduction reaction happens in the cathodic path is depressed by a formation of insoluble compounds precipitating on the cathodic sites rather than a passivation oxide film. In this way, the effective cathode area is decreased and the corrosion is retard or even prevented[13].

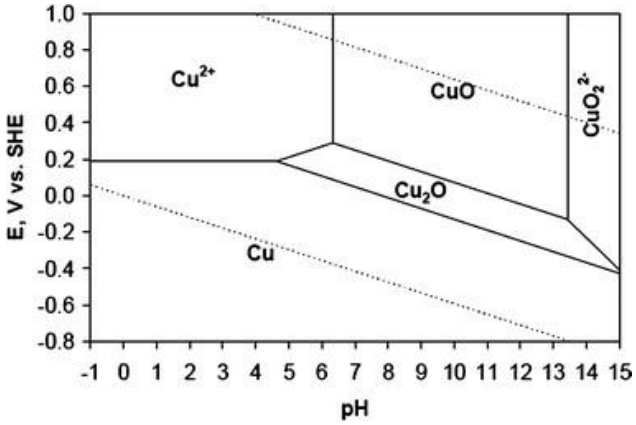

Figure 1.1 The Pourbaix diagram of copper

Initially, inorganic corrosion inhibitors, such as nitrites, nitrates and chromates, were more widely employed to protect metals and alloys from corrosion in the corrosive media. However, because of the more restrictive environmental regulations as well as the toxicity on human lives and natural environment of most inorganic corrosion inhibitors, new environmentally friendly organic compounds are required to be investigated and developed to replace inorganic corrosion inhibitors[14]. At the same time, due to the high efficiency of organic molecules to impede corrosion (related to their self-assembled mono-layers), the formed nano-metric-thickness layer and the ease of applications (especially on the situations contained very complicated shaped objects), organic inhibitors have been turned into attractive candidates for the corrosion inhibitive potential in various corrosive media[14].

As stated by Fouda that the corrosion inhibition efficiency of an organic inhibitor is mainly related to its capacity to be adsorbed on the material surface to form interfacial bonds when water molecule exchange happens at the corroding interface[15]. As for how organic inhibitors are adsorbed on the material surface, following four different adsorption mechanisms are widely considered[16]:

(1) Electrostatic interaction between the charged material surface and the charge of the inhibitor (physisorption);
(2) Interaction between material surface and unshared electron pairs of the inhibitor (chemisorption);
(3) Interaction between material surface and π-electron;
(4) A combination of the first and third type

Amongst these four types of adsorptions, physisorption and chemisorption are mainly considered in this master thesis. For physisorption, the interfacial interaction is merely fulfilled by electrostatic force between the electric charges at the specimen/solution interface and ionic charges or dipoles on the adsorbed species, while for chemisorptions, charge sharing or charge transfer is involved in the interfacial interaction with material surface[16]. Therefore, physisorption has a relative low heat and adsorption energy compared with chemisorptions and is usually stable at relative

low temperature for relative short working time[16].

For chemisorption, however, since charge sharing or charge transfer is involved, the key function of heteroatoms or donor atoms which have the ability of giving electrons is non-negligible in the formation of coordinative bonds at the specimen/solution interface. Nitrogen, sulfur, oxygen and sulfur atoms are typical donor atoms. For copper and copper alloys, because of the vacant d-orbital of copper ions, coordinative bonds are more easily to be formed by accepting electrons from electrolyte atoms. Therefore, the attendance of donor atoms in the organic compound molecules can increase their chemisorption probability and their inhibition action can be strengthened[15]. Namely, organic inhibitors with more donor atoms are more easily to be chemisorbed and have a higher inhibition theoretically. Nevertheless, as some recent research reports, the chemisorption of organic inhibitors is not only depends on the donor atoms (e.g. their density and orbital characters), but also depends on the physicochemical and electronic properties of these organic molecules, such as their functional groups, the steric effects and etc[17]. In other word, donor atoms in the organic inhibitor molecules cannot completely decide the chemisorption or the inhibition of one organic inhibitor, other factors are also important.

Studies on how organic inhibitors being adsorbed on the surface of the tested material (by electrostatic interaction or charge transfer) and how the interfacial interactions change with time are main research purposes of this master thesis.

1.4 Aims of this master thesis

This master thesis mainly had two stages of research. In the first stage, organic corrosion inhibitors were pre-selected by comparing on their inhibition effects on copper and brass. Then, those with better inhibition effect on the tested materials with higher inhibition efficiencies were chosen and used in the second stage of detailed analysis on their interaction mechanisms.

Chapter 2 EXPERIMENTS and MATERIALS

This thesis is divided into two parts for different research purposes. In the first stage of pre-selection of organic corrosion inhibitors, Linear Polarization Resistance (LPR) measurement was employed to provide valuable information of the polarization resistances of immersed specimens as well as the inhibition efficiencies of inhibitors on specimens. In the second stage of detailed analysis on the chosen inhibitors, Electrochemical Impedance Spectroscopy (EIS) and Fourier Transform Infrared (FTIR) Spectroscopy were used to investigate the interaction mechanisms of inhibitors on copper and brass. Open circuit Potential (OCP) measurement was used in both stages.

Furthermore, in these two stages of research, different specimens were used because of the Kretschmann geometry in FTIR spectroscopy and limitations of physical vapor deposition (PVD). But zinc was included in both stages since it is a principal alloying element of brass. Meantime, although three-electrode corrosion cell was applied for electrochemical measurements in both stages, different equipments were employed. The choice of equipments depended on specimens.

2.1 Open Circuit Potential measurement

2.1.1 Introduction of OCP measurement

Open circuit potential (OCP), which is also known as the open circuit voltage (OCV), is the electrical potential difference between the working electrode (the tested material) and the reference electrode when the circuit involving no external current[18]. The shift of the open circuit potential of the working electrode, which is caused by the change of capacitance of the dielectric layers while the chemical oxide is growing in the solution, can be collected by Open Circuit Potential (OCP) measurement, so it is a

useful electrochemical method for the study of corrosion inhibitors[19]

When a metal or alloy is exposed to an aggressive solution with an organic corrosion inhibitor in certain concentration, a protective polymer thin film will form on the specimen surface by the interfacial interaction between the specimen and the organic inhibitor. Because of the different electrical properties between the specimen and this polymer layer, the shift of the open circuit potential can reflect the chemical state of the specimen and evaluate the durability of its protective polymer layer. In other words, OCP measurement is sensitive to detect different conditions of the working electrode, such as its chemical state (oxidation or reduction) and the adsorption of other chemicals species[20]. Furthermore, compared with other long-term exposure tests, OCP measurements can be performed in relative short time, so it is very helpful to save time for electrochemical experiments[21].

In addition to the evaluation of the tested material and its protective polymer mono-layer, the main purposes of OCP measurement in this master thesis are allowing the specimen to be stabilized under the open circuit condition and monitoring the corrosion behavior of the specimen surface. Only when the immersed specimen maintains in a stable state, following electrochemical measurements including Linear Polarization Resistance (LPR) measurement and Electrochemical Impedance Spectroscopy (EIS) could work accurately. Generally, the time for the specimen to achieve its stable state is at least 1 hour. The stable or quasi-steady state open circuit potential at the end of the stabilization state is denoted as the steady state open circuit potential E_{ocp} or corrosion potential E_{corr}. After OCP measurement, a function of time is measured versus the open circuit potential of the specimen, so it is also an accurate way to count the exposure time.

2.1.2 Experimental procedure of OCP measurement

As mentioned above that a three-electrode corrosion cell was employed in the OCP measurement as well as in the following electrochemical measurements. Although different equipments were used for different specimens in two stages of research, their working principle kept unchanged. The working schematic diagram of a three-electrode corrosion cell is shown in the figure 2.1, where WE represents the working electrode (copper, copper-zinc alloys and zinc), RE represents the reference electrode (Ag/AgCl) and CE represents the conventional counter electrode (a stainless steel sheet with around 2 cm^2 surface area for copper and zinc or a graphite rod for copper-zinc alloys). What should be noticed is that in the three-electrode corrosion cell, the potential is measured between the reference electrode and the working electrode, while the current is measured between the counter electrode and the working electrode.

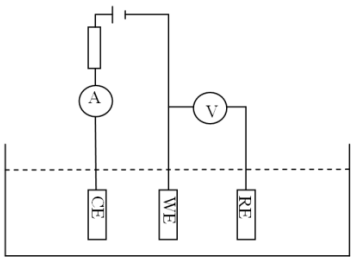

Figure 2.1 Working schematic diagram of a three-electrode corrosion cell

In this master thesis, Solartron SI-1286 was used for OCP measurement.

2.2 Linear Polarization Resistance measurement

2.2.1 Introduction of LPR measurement

Linear Polarization Resistance (LPR) measurement is a widely used method to obtain the corrosion rate and the linear polarization resistance (R_p) of specimens directly. The working schematic diagram of the equipment used for LPR measurement can also be indicated by the figure 2.1. General, the linear polarization resistance is defined as the difference of real impedances at the lower and the higher frequency, and it can be calculated as the ratio between the applied voltage △E (shifted potential from the corrosion potential E_{corr}/steady state open circuit potential E_{ocp}) and the current density △i when the tested material is slightly polarized from the corrosion potential E_{corr}/steady state open circuit potential E_{ocp} [22-23]. It is indicated in the equation 2.1. According to the equation 2.2 and 2.3, R_p is inversely proportional to the corrosion current density i_{corr}:

$$R_p = \left(\frac{\Delta E}{\Delta i}\right)_{\Delta E \to 0} \quad \text{eq. 2.1}$$

$$i = \frac{I}{A} \quad \text{or} \quad i_{corr} = \frac{I_{corr}}{A} \quad \text{eq. 2.2}$$

$$R_p = \frac{\beta_a \beta_c}{2.3 \times i_{corr}(\beta_a + \beta_c)} \quad \text{eq. 2.3}$$

where I_{corr} is the corrosion current, A is the polarized surface area of the specimen, β_a and β_c are the anodic and cathodic Tafel constants.

Combining with the fact that the corrosion rate is proportional to i_{corr}, linear polarization resistance R_p is inversely proportional to the corrosion rate. Therefore, the greater the R_p, the slower the corrosion process is.

The linear polarization resistance R_p can also be understood by a simple equivalent circuit shown in the figure 2.2, where R_s represents the solution resistance (the electrical resistance of the corrosive solution or aggressive surrounding environment) and C_{dl} is a double layer capacitance (provided by charged ions on the surface of specimens). For copper and copper alloys exposed to the aggressive environment, if there is no corrosion inhibitor or protection coating, corrosion can happen easily on the materials surface. This process is a dynamic electrochemical process, during which ions exchanges between the active (anodic) and the passive (cathodic) locations. It can be represented by the equivalent circuit shown in the figure 2.2 which consists of different elements including the linear polarization resistance R_p. In this equivalent circuit, R_p reflects the ease with which charged ions can leave the materials surface and enter the aqueous solution, so this explanation accords with the mathematically relationship between R_p and the corrosion rate mentioned above. This equivalent circuit is also significant to explain physical meanings of various elements in the corrosion process and linked with Electrochemical Impedance Spectroscopy (EIS) which will be discussed in detail later.

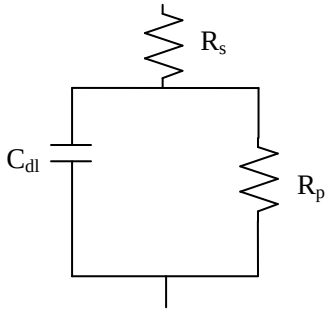

Figure 2.2 A simple equivalent circuit of corrosion

At the same time, LPR measurement is also an efficient approach to study the inhibition efficiency (η%) of a corrosion inhibitor on the tested specimen in a certain aggressive environment, as presented in the equation 2.4[22,24]:

$$\eta\% = \frac{\frac{1}{R_p} - \frac{1}{R_p'}}{\frac{1}{R_p}} \times 100\% = \left(\frac{R_p' - R_p}{R_p'}\right) \times 100\% \qquad \text{eq. 2.4}$$

where R_p and R_p' represent the polarization resistance of the sample in the absence and presence of the corrosion inhibitor, respectively.

2.2.2 Experimental procedure of LPR measurement

LPR measurement was employed in the first stage of inhibitors pre-selection to provide information on the inhibitions and inhibition efficiencies of different inhibitors. In this way, those with better inhibition effects can be chosen for the

following investigation on their interaction mechanisms. As mentioned in the 2.1, the specimen was required to be immersed in the test solutions for at least 1 hour in order to achieve its stable state. Then, LPR measurement was carried out by recording the electrode potential ±0.015V around the E_{corr} or E_{ocp} starting from the cathodic potential. The scan rate was defined at 10mV/min. Based on the surface area of the specimen exposed to the tested solution (2.835 cm^2 for copper and zinc, 0.95 cm^2 for copper-zinc alloys), the linear polarization resistance R_p of each specimen can be calculated from the slope of the obtained current-potential curves shown in the figure 2.3 with the equation 2.5:

$$R_p = \frac{R_{p1}+R_{p2}}{2} \qquad \text{eq. 2.5}$$

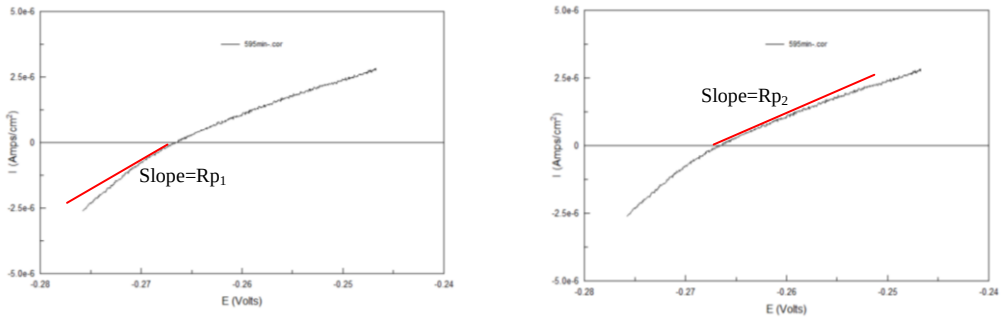

(a) Rp_1 (b) Rp_2

Figure 2.3 The schematic diagram of the calculation method of Rp

In this master thesis, Solartron SI-1286 was used for LPR measurement.

2.3 Electrochemical Impedance Spectroscopy

2.3.1 Introduction of EIS

Electrochemical Impedance Spectroscopy (EIS) is a powerful non-destructive method to investigate the corrosion kinetics and corrosion protection mechanisms, especially for the cases of corrosion protection provided by corrosion inhibitors, polymer coatings and anodic layers. The impedance reflects the tendency of a circuit to resist (or impede) the flow of an alternating electrical current (AC) in a defined electrochemical system.

EIS was employed in the second stage of analysis on the detailed analysis on the interaction mechanisms of organic inhibitors. The working schematic diagram of EIS is shown in the figure 2.4 with a working electrode (WE), a reference electrode (RE)

and an inert counter electrode (CE). Similar as what discussed in the Chapter 2.1, only the impedance between the reference electrode and the working electrode and the current between the counter electrode and the working electrode are measured during EIS. Normally, there is not only one path for current to travel in a given experimental system, but the current will always choose the one or several closely matched predominant paths which has (or have) the least resistance between two electrical electrodes. Therefore, EIS can only measure the least impedance of the predominant path (or paths).

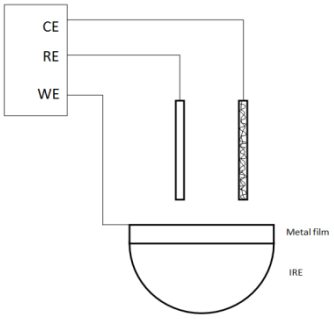

Figure 2.4 Working schematic diagram of EIS

During EIS, periodic sinusoidal voltage signals which can perturb the electrically conductive specimens surface is applied, then a sine wave with a shift in phase angle (Φ) and a changed amplitude responses. It is demonstrated in the figure 2.5. EIS collects this electrochemical response and reflects the dielectric properties of a corrosive media as a function of frequency denotes:

$$U(\omega) = U_0 \cdot \sin(\omega t) \qquad \text{eq. 2.6}$$

$$I(\omega) = I_0 \cdot \sin(\omega t + \varphi) \qquad \text{eq. 2.7}$$

$$Z(\omega) = \frac{U(\omega)}{I(\omega)} = Z_{re}(\omega) + j \cdot Z_{im}(\omega) = Z_A(\cos\varphi + j \cdot \sin\varphi) \qquad \text{eq. 2.8}$$

where U(ω) is the input voltage, I(ω) is the output measured current and Z(ω) is the complex impedance of the system calculated based on the Ohm's law.

Hence, impedance is a complex quantity with a real or in-phase part (Z_{re} or Z) and an imaginary or out-phase part (Z_{im} or Z'). The data collected by EIS can be represented in either Nyquist plot (plotting the real part Z_{re} or Z as X-axis against the imaginary part Z_{im} or Z' as Y-axis) or Bode plot (plotting the logarithmically frequency as X-axis against the real part Z_{re} or Z as Y axis). Nyquist plot and Bode plot are shown in the figure 2.6, both of them can show direct information of corrosion behaviors of specimens. In both Nyquist plot and Bode plot, the impedance at high frequency is equal to the ohmic resistance or the solution resistance ($|Z| = R_\Omega/R_s, R_\Omega/R_s$ mainly reflects the properties of the surrounding environment, so it is usually seen as unchanged in the same experimental system), while that at low frequency is given as the sum of the polarization resistance and the ohmic resistance ($|Z| = R_\Omega +$

R_P or $|Z| = R_s + R_P$). What is important for Nyquist plot is that the high frequency end of the semi-circle is on the left side of the X-axis, while the low frequency end is on the right side.

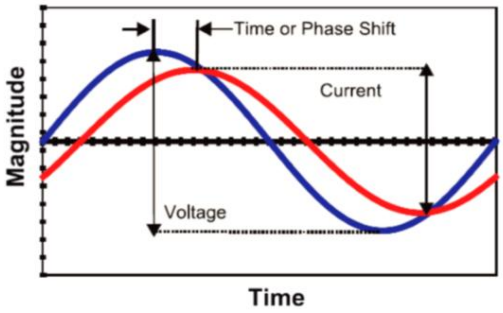

Figure 2.5 The current and voltage as a function of time[25]

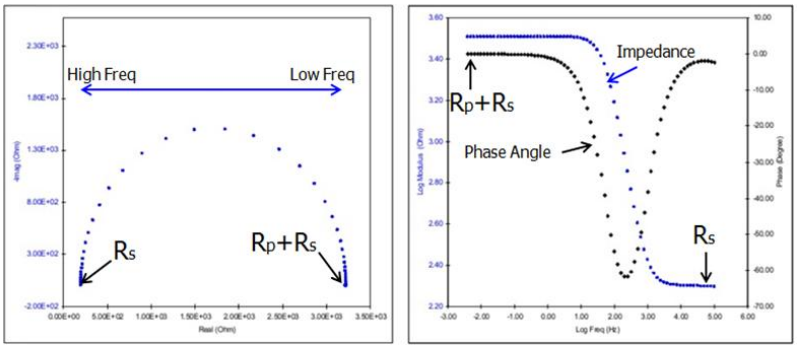

Figure 2.6 Nyquist plot (left) and Bode plot (right)

Generally, attention will not be paid to the coating system directly before the failure caused by corrosion happens at the metal/coating interface. After the failure happens, however, an equivalent circuit mentioned in the Chapter 2.2 with different elements including R_s and C_{dl} can be modeled to provide important physical information of the failed coating system[26]. This equivalent circuit is a model based on the understanding of this electrochemical system which represents a complex phenomenon transferring chemical, physical, electrical and even mechanical components into purely electrical terms. So a suitable equivalent circuit can be used to describe the experimental data and predict the system behaviors. However, it is important to note that the best fit equivalent circuit model may loss its physical meanings because of the ambiguity of involved ideal elements[27]. Therefore, priority attentions in this master thesis should be paid to establishing a meaningful equivalent circuit according to EIS in order to explain the electrochemical failure at the metal/coating interface.

2.3.2 Experimental procedure of EIS

In this master thesis, EIS were performed from 30000 Hz to 0.01 Hz with sinusoidal

amplitude of 5 mV using multisine measurements for low frequencies. Solartron SI-1255 was used for EIS.

2.4 Fourier Transform Infrared Spectroscopy

2.4.1 Introduction of FTIR spectroscopy

Fourier Transform Infrared (FTIR) Spectroscopy is a high-tech technique commonly used to obtain an infrared spectrum of absorption or emission behaviors of a solid, liquid or gas. As mentioned in the Chapter 1.3 that the absorption behavior of an organic inhibitor is a major determining factor of its inhibition effect, so this master thesis mainly focused on the infrared spectrum of absorption behavior of organic inhibitors. The absorption process only happens when the frequency of the infrared light is equal to the vibration frequency of a bond or a functional group of one organic molecule, combined with the fact that the vibration frequency is a characteristic of a specific molecule, it is reasonable to collect information of vibration states of various molecules according FTIR spectrum.

In order to study in detail on the interaction mechanism of an organic inhibitor in the second stage of research, both ex-situ and in-situ FTIR spectroscopy were employed. Ex-situ FTIR spectroscopy can offer the information about the absorption type (physisorption or chemisorption) of an organic inhibitor. If it is chemisorption, ex-situ FTIR spectroscopy can also provide information about which functional group of this inhibitor contributes to the absorption process. In-situ FTIR spectroscopy can indicate the interfacial interaction of one organic inhibitor with the specimen, namely, it can show the change of absorbed functional groups with time. In this way, the information about the formation or the break of an interfacial bond between the inhibitor molecules and the specimen surface can be transferred by in-situ FTIR spectroscopy.

2.4.2 Experimental procedure of FTIR spectroscopy

Since both in-situ FTIR and EIS measurements can reflect the interaction mechanism of an inhibitor on specimens, every time when in-situ FTIR spectroscopy was measuring to get an absorption behavior infrared spectrum, EIS was working at the same time for important information about the physical meanings of different elements during the corrosion process. Similarly, OCP measurement was also employed in this stage to allow specimens to be stabilized under the open circuit conditions.

In this master thesis, Nicolet 6700 was used for FTIR spectroscopy. Because of the limitation of the instrument, the spectral range of in-situ FTIR and ex-situ FTIR measuring mode for non-dissolved inhibitors was limited between 500 and 4000 cm^{-1}, while that of ex-situ FTIR measuring mode for dry specimens was limited between 650 and 4000 cm^{-1}. Meantime, attention was paid to cooling down the instrument by liquid nitrogen (around -196 ℃) before use. In this way, the noise caused by thermally excited current carriers could be reduced dramatically.

2.5 Specimens

As mentioned above that there were two stages of analysis with different research purposes in this master thesis. In the first stage of inhibitors pre-selection, OCP and LPR measurements were employed to provide necessary information about inhibition behaviors and inhibition efficiencies of inhibitor candidates on copper and brass. Then, those with higher inhibition were chosen. In the second stage, the chosen inhibitors were analyzed in detail on their interaction mechanisms on tested materials by means of OCP, EIS and FTIR measurements.

On the basis of the specific requirements of specimens used in in-situ FTIR spectroscopy which will be detailed discussed in the following chapter, specimens used in these two stages were different. Because zinc is an important metal component in the brass, pure zinc was also included as one of specimens in both stages in order to obtain a more complete conclusion.

2.5.1 Specimens for inhibitors pre-selection

Before the detailed study on the interaction mechanisms of organic corrosion inhibitor candidates on the copper and brass, their inhibition behaviors and inhibition efficiencies in the same aggressive environment were firstly investigated and compared with the help of OCP and LPR measurements.

In this procedure, pure copper, 10% Zn copper alloy, 30% Zn copper alloy, 40% Zn copper alloy and pure zinc were studied as specimens. Their microstructures are shown in the figure 2.7. Pure copper and pure zinc were cut into 30 mm×30 mm flat sheets, while cylindrical brass with the thickness of 1 mm and the diameter of 11 mm were connected with a copper wire in the back side and embedded in the resin. This copper wire was used for the electrical connection for electrochemical measurements, so its electrical connection with alloys was significant and required to be tested initially.

Before the measurements, all specimens were polished mechanically with different grades of silicon carbide paper (from 320 to 4000) firstly. Then, they were degreased with enthanol in an ultrasonic vibrator for 3 min. After double rinsed with distilled water, specimens were dried with nitrogen gas and could be used for OCP and LPR measurements.

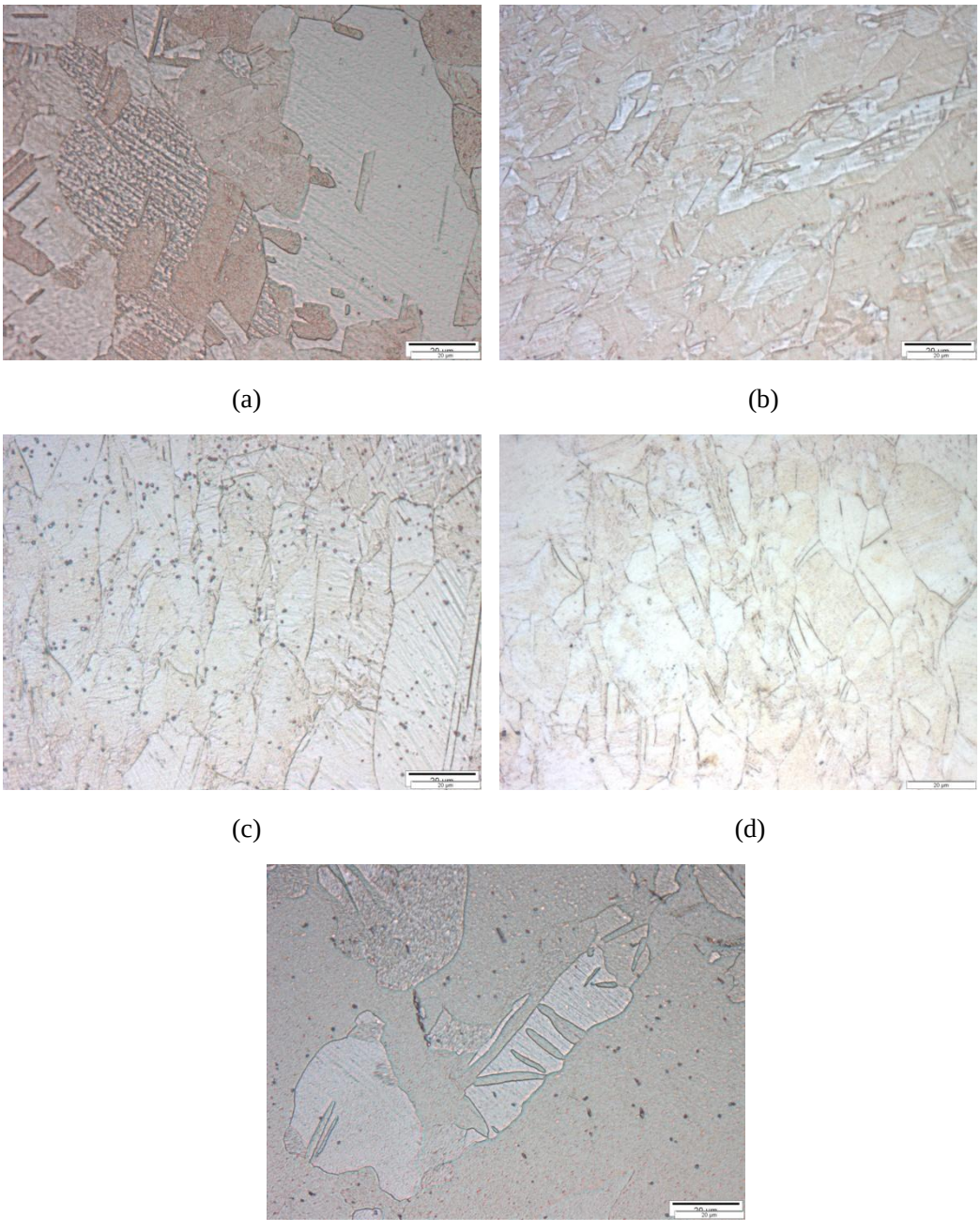

(a) (b)

(c) (d)

(e)

Figure 2.7 The microstructures of specimens for inhibitors pre-selection: (a) Pure copper; (b) 10% Zn copper alloy; (c) 30% Zn copper alloy; (d) 40% Zn copper alloy; (e) pure zinc

As mentioned above that three-electrode cell was employed for electrochemical measurements. In the first stage of inhibitors screening preformed by OCP and LPR

measurements, a flat cell was used for the pure copper and pure zinc flat sheet. Before OCP and LPR measurements, the flat cell was required to be assembled in the way shown in the figure 2.8 (a). The connection between separated components of a flat cell should keep close-knit in order to avoid leakage of solution.

However, the flat cell cannot be employed for embedded brass specimens because of the back-side-connected copper wire. Alternatively, equipment shown in the figure 2.8 (b) was used. For this three-electrode corrosion cell, the working electrode (the embedded brass specimens) was put in a face-down position and required to be completely immersed in the electrolyte.

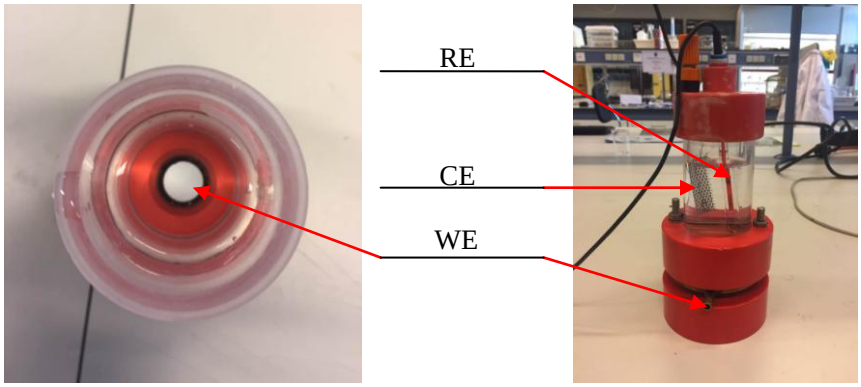

(a)

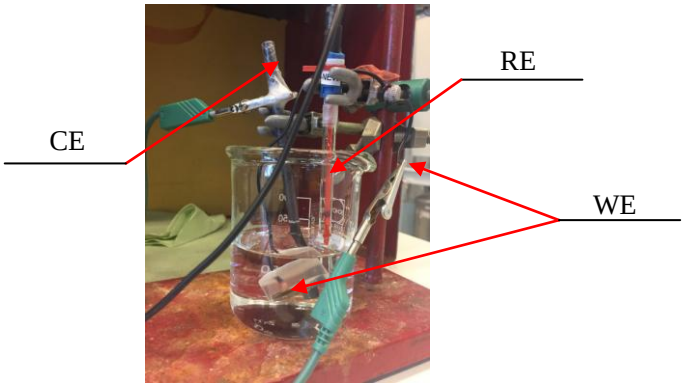

(b)

Figure 2.8 The electrochemical system of OCP and LPR measurements: (a) for pure copper or pure zinc, (b) for brass, WE: working electrode (pure copper or pure zinc for (a) and brass for (b)), RE: reference electrode (Ag/AgCl), CE: counter electrode (stainless steel for copper and zinc and graphite rob for brass)

2.5.2 Specimens for detailed analysis of inhibitors

After comparing the corrosion inhibition behaviors and inhibition efficiencies of different corrosion inhibitors in the same aggressive environment, OCP, EIS and FTIR measurements were applied to further analyze on the interaction mechanism of the

chosen inhibitors.

As mentioned in the Chapter 2.4 that both in-situ FTIR and ex-situ FTIR spectroscopy were employed in this stage to provide more comprehensive information. The Kretschmann geometry of in-situ FTIR spectroscopy is shown in the figure 2.9. According to the Kretschmann geometry, an internal reflection element (IRE), which is also known as the attenuated total reflectance (ATR) crystal, was included. Because of the special optical properties, this ATR crystal is significant to ensure the incident infrared light be reflected back to the detector. In this master thesis, a Ge crystal was employed as the ATR crystal in in-situ FTIR spectroscopy. The Ge crystal is shine with black or dark grey metallic luster, it is not transparent and its refractive index is around 4. Before the deposition, the Ge crystal was rinsed in acetone and ultrasonically cleaned in ethanol for 5 min in order to remove unavoidable physical and chemical dirt from the surface. Afterwards, it was cleaned ultrasonically by Milli-Q water (MQ water) for 5 min and repeated for another time. Then, it was rinsed in MQ water and dried. The Ge crystal which had been used for the last in-situ FTIR spectroscopy was cleaned in the same way in order to remove the dirt as well as the remaining chemical inhibitor.

Based on the working principle of FTIR spectroscopy, it is compulsory for the incident infrared light to arrive at the specimen/solution interface and be reflected back to the detector. However, the penetration depth of the incident infrared light is limited, if the metal film is too thick, the infrared light cannot be reflected to the detector or even cannot arrive at the specimen/solution interface. Hence, the specimen and ATR crystal are required to contact closely. This direct contact can only be carried out by physical vapor deposition (PVD). PVD, known as a widely used vacuum deposition method to deposit a metal film on a substrate surface, can produce a metal vapor in the vacuum. In this way, the thickness of the deposited metal film can be controlled in the scale of nanometer.

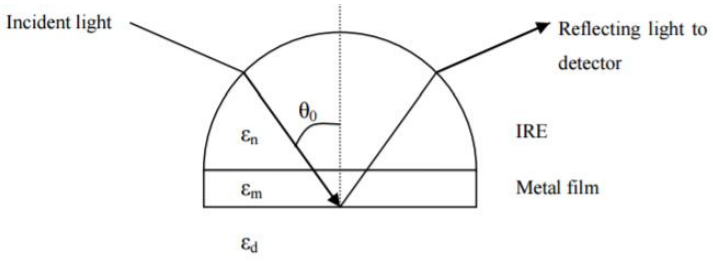

Figure 2.9 The Kretschmann geometry

The evaporator used in PVD to deposit metal or alloy thin films on the Ge crystal surface was Rack Type Vacuum Evaporator VCM 600-SP3. During PVD, the Ge crystal was placed in a face-down position in order to avoid metal particles settling on the top surface of ATR crystal which was used for deposition. In this way, a relative uniform deposition could be achieved and a high quality deposited thin film could be

obtained. Meantime, the bottom and the side of the ATR crystal were covered by alumina foil before being put into the evaporator in order to prevent metal vapor depositing on these surfaces.

The thickness of this deposited thin film on the Ge crystal is one of the most important factors for in-situ FTIR spectroscopy. On the one hand, it can influence the response of FTIR spectroscopy because of the limited penetration depth of the incident infrared light. The higher the thickness of this film, the lower the response as well as the signal to noise ratio. Thus, the quality of the information provided by in-situ FTIR spectroscopy as well as the credibility of results will decrease. On the other hand, attention should also be paid to the quality of this deposited film. Only when this thin film is thick enough, it can be continuous, so the surface can be electrically conductive. Overall, trail tests should be done in order to get a suitable thickness of this deposited thin film. Based on the experiences obtained from the internship project, the thickness of the deposited films on the Ge crystal was defined at about 13.3 mm.

Other than the thickness of the deposited thin film, the deposition rate of metals is also a very important factor for getting a dense and uniform film with high quality. In order to ensure the comparability of various films deposited in different deposition processes, the deposition rate was maintained at around 0.2-0.4 Å/s. What should be noticed is that the deposition process of pure metal (pure copper or pure zinc) thin films is different from that of copper-zinc alloys thin films. For pure metal thin films, only one kind of metal vapor, copper vapor or zinc vapor, is needed for deposition, so only one heat source is required to be controlled in order to maintain the deposition rate at around 0.2-0.4 Å/s. However, both copper and zinc vapors are required for the deposition process of copper-zinc alloys thin films. Because of the different melting temperatures of copper and zinc, it is difficult to deposit an alloy thin film with a precise content ratio by PVD. But a copper-zinc alloy thin film with 50% Cu+50% Zn (volume ratio) can be roughly achieved (controlled the heat source of copper base in order to increase its deposition rate to around 0.1-0.2 Å/s initially, then controlled the heat source of zinc base to increase the total deposition rate to around 0.2-0.4 Å/s, so the deposition rate of both copper vapor and zinc vapor can be seen as equal around 0.2 Å/s and the volume ratio of copper and zinc deposited on the Ge crystal surface can be seen as 1:1). Therefore, the specimens used in the second stage of detailed analysis of the chosen inhibitors were pure copper, 50% Zn copper alloy and pure zinc thin film made by PVD.

As mentioned in the Chapter 2.3.1 that a sinusoidal voltage is applied during EIS and the Chapter 2.4.2 that EIS and in-situ FTIR spectroscopy were working at the same time. Therefore, this deposited metal or alloy thin film should be electrically conductive in order to transport current between the working and reference electrodes. That is also the reason why the ATR crystal was required to be cooled down after PVD (avoiding the formation of a non-conductive oxide film caused by the high

temperature). In order to ensure the deposited thin film was continuous and did not oxidize after deposition, the voltage of this thin film was measured before assembling the three-electrode corrosion cell. The voltage meter used in this procedure was Velleman DVM 8264.

Before OCP, EIS and in-situ FTIR measurements, specimens were assembled in a three-electrode corrosion cell shown in the figure 2.10. The electrochemical structure is shown in the figure 2.11. Same as the equipments used for the first stage of screening, the connection between separated components of a cell should also keep close-knit to avoid leakage of solution. Meanwhile, a copper tape with a length of around 10 cm was used for the connection of the electrically conductive metal or alloy thin film with the instrument.

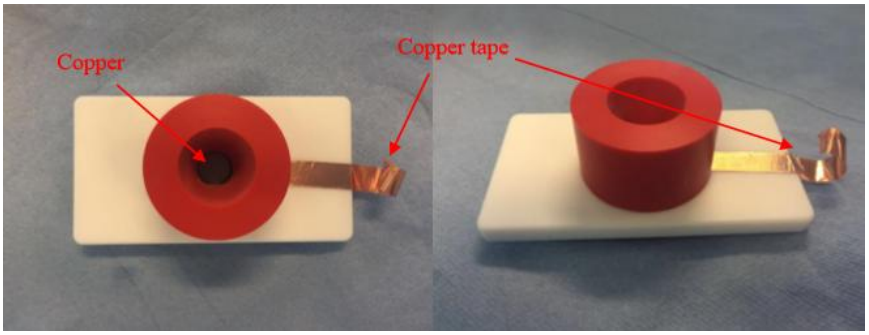

Figure 2.10 The equipment (cell) for EIS and in-situ FTIR measurements

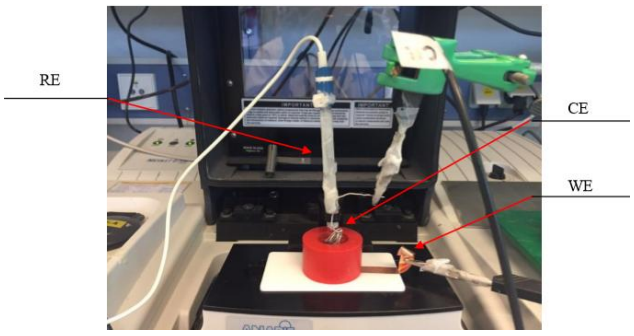

Figure 2.11 The electrochemical structure of EIS and FTIR measurements, WE: working electrode (pure copper thin film or brass thin film), RE: reference electrode (Ag/AgCl), CE: counter electrode (stainless steel)

For ex-situ FTIR spectroscopy, however, three-electrode corrosion cell was not required.

2.5.3 Cleanness of equipments

In order to ensure the accuracy of results and reduce the factors that can affect the experiments, it is necessary to ensure the used equipments (separated components of a cell or a beaker) and electrodes (reference electrodes and counter electrodes) are clean

without dirt or remaining chemical inhibitors. Therefore, they were cleaned before and after every measurement. Nevertheless, different kinds of equipments needed different cleaning approaches, even different components of one cell had different cleaning methods.

For electrochemical measurements in both stages of analysis mentioned above, the reference electrodes and the counter electrodes were rinsed by water and then MQ water. The flat cell used for pure copper and pure zinc in inhibitors screening (by OCP and LPR measurement) was cleaned by water, while the beaker used for brass was rinsed in ethanol and then water. As for the separated components used for EIS and in-situ FTIR measurements, they were rinsed in ethanol and cleaned ultrasonically in ethanol for 10 min. Then, after rinsing in MQ water, they were dried and clean without physical and chemical dirt.

2.6 Inhibitors

In the past few decades, benzotriazole ($C_6H_5N_3$) was used as the most effective organic inhibitor on copper and copper alloys in the corrosive agent[16]. But in recent years, various organic compounds such as azoles, amines, amino acids have been extensively considered as a less toxic but more effective alternatives of benzotriazole[28].

In this master thesis, three different kinds of azoles inhibitors, i.e. imidazole, 2-mercapto-benzimidazole (MBI) and 2-mercapto-1-methyl-benzimidazole (1H-HB-2T), were compared and investigated on their corrosion inhibition effects and interaction mechanisms on copper and brass. 3 wt% sodium chloride aqueous solution (NaCl solution) was used as the aggressive media. The concentration of these three inhibitors in the 3wt% NaCl aqueous solution was same as 1mmol/100ml.

2.6.1 Imidazole

Imidazole is an organic compound with the formula $C_3H_4N_2$. According to its structure shown in the figure 2.12, imidazole is an aromatic heterocycle. In chemistry, imidazole can be classified as a diazole.

Amongst these three inhibitor candidates studied in this master thesis, imidazole has the simplest structure. Combining with the chemisorption mechanism mentioned in the Chapter 1.3, two non-adjacent nitrogen atoms can be seen as donor atoms..

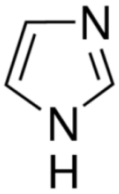

Figure 2.12 The structure of imidazole

2.6.2 2-mercapto-benzimidazole

2-mercapto-benzimidazole (MBI or 2HB) is a chemical compound from the group of benzimidazoles with the formula $C_7H_6N_2S$. Generally, MBI can present in two different tautomeric forms with the hydrogen atom moving between the nitrogen atom and the sulfur atom. This process is shown in the figure 2.13.

Compared with the simple structure of imidazole, MBI has one more kind of donor atom, nitrogen atom and sulfur atom.

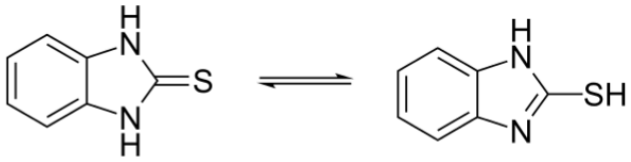

Figure 2.13 The structure of 2-mercapto-benzimidazole (MBI or 2HB)

2.6.3 2-mercapto-1-methyl-benzimidazole

2-mercapto-1-methyl-benzimidazole (1H-HB-2T) is a chemical compound from the group of benzimidazoles with the formula $C_8H_8N_2S$. It also has an alternative name, 1-methyl-1H-benzimidazole-2-thiol. As shown in the figure 2.14 the structure of 1H-HB-2T is the most complex amongst these three inhibitor candidates.

Same as MBI, 1H-HB-2T contains two different donor atoms, nitrogen atom and sulfur atom. In addition to this extra donor atom, 1H-HB-2T also has a methyl group which occupies the position of a hydrogen atom.

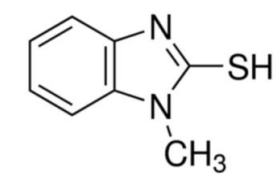

Figure 2.14 The structure of 2-mercapto-1-methyl-benzimidazole (1H-HB-2T)

Chapter 3 RESULTS and DISCUSSIONS

As mentioned above that three kinds of organic corrosion inhibitors were studied in this master thesis. Initially, LPR measurement was employed to compare their inhibition behaviors on copper and zinc-copper alloys. Then, those with higher inhibition efficiencies were chosen for the following research on their interaction mechanisms by means of EIS and FTIR measurements.

3. 1 Pre-selection of inhibitors

Since the polarization resistance of a specimen is inversely proportional to the corrosion rate, it can reflect the inhibition effect of a corrosion inhibitor. In other words, the higher the polarization resistance, the better the inhibition effect of the inhibitor is. In the inhibitors pre-selection stage of this master thesis, 1 mmol/100ml imidazole, 2-mercapto-benzimidazole (MBI) and 2-mercapto-1-methyl-benzimidazole (1H-HB-2T) were compared and screened based on the polarization resistances of exposed specimens (pure copper, 10% Zn copper alloy, 30% Zn copper alloy, 40% Zn copper alloy and pure zinc).

LPR measurement was used to collect the polarization resistances of exposed specimens in 100 hours (collected after 2 hours, 5 hours, 10 hours, 20 hours, 30 hours, 40 hours, 50 hours, 60 hours, 70 hours, 80 hours, 90 hours and 100 hours), so the changes of the polarization resistances could be found and provided valuable information of interactions between specimens and inhibitors. The detailed experiment set is attached in the Appendix A based on the fact that the time needed for measuring the polarization resistance of one specimen was around 5 min. The changes of the polarization resistances of exposed specimens in 100 hours are shown in the figure 3.1.

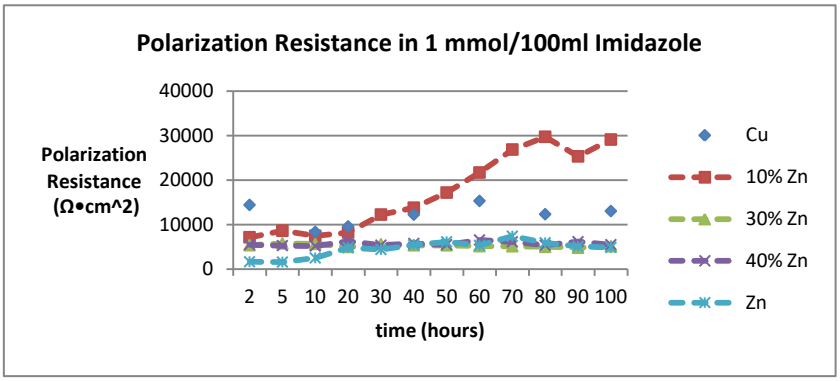

(a)

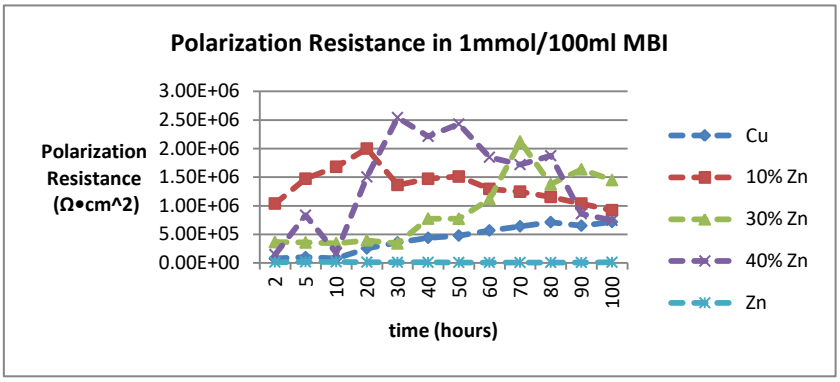

(b)

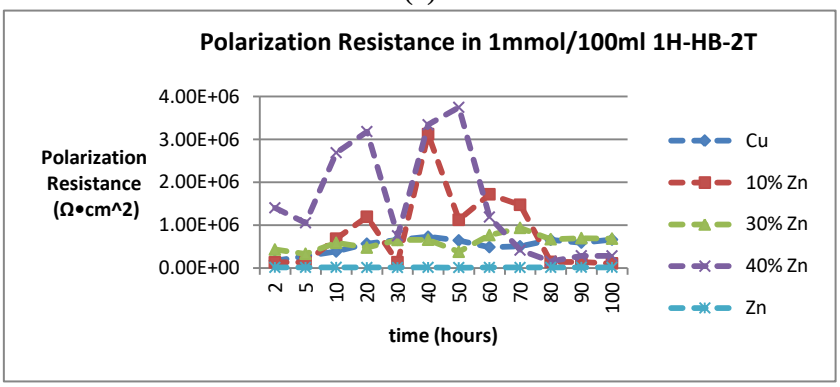

(c)

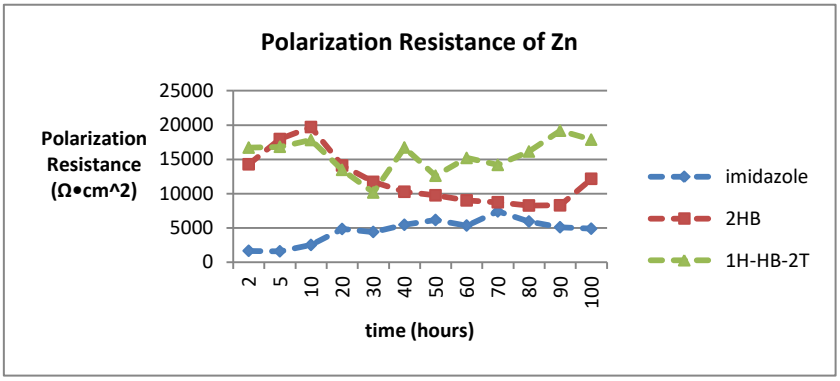

(d)

Figure 3.1 Polarization resistances of specimens immersed in 1 mmol/100ml (a) imidazole, (b) MBI, (c) 1H-HB-2T; (d) Polarization resistances of zinc immersed in 1 mmol/100ml imidazole, MBI and 1H-HB-2T

In the figure 3.1, important information can be provided by the Y-axis which corresponds to the polarization resistances of specimens. The polarization resistances of specimens immersed in 1 mmol/100ml imidazole had the lowest value in 100 hours compared with that of specimens immersed in MBI and 1H-HB-2T with the same concentration. In other words, when the concentration was 1 mmol/100ml in NaCl aqueous solution, imidazole had the worst inhibition effects on copper and brass amongst these three inhibitors. The lower inhibition of imidazole can be further proved by the inhibition efficiencies (η%) of three candidates calculated from the equation 2.4,

$$\eta\% = \frac{\frac{1}{R_p} - \frac{1}{R_p'}}{\frac{1}{R_p}} \times 100\% = \left(\frac{R_p' - R_p}{R_p'}\right) \times 100\% \qquad \text{eq. 2.4}$$

where R_p and R_p' represent the polarization resistance of the sample in the absence and presence of the corrosion inhibitor, respectively.

The changes of inhibition efficiencies of 1 mmol/100ml imidazole, MBI and 1H-HB-2T on specimens in 100 hours are shown in the figure 3.2. According to the figure 3.2, the inhibition efficiencies of 1 mmol/100ml imidazole were relative low compared with that of MBI and 1H-HB-2T with the same concentration. It meant that its inhibitions on copper and brass were lower than that of MBI and 1H-HB-2T. Furthermore, when 30% Zn copper alloy and 40% Zn copper alloy were exposed to the 1 mmol/100ml imidazole, negative inhibition efficiencies appeared. Therefore, for 30% Zn copper alloy and 40% Zn copper alloy, imidazole did not work well and its corrosion protection was weaker than that provided by other anti-corrosion mechanisms (e.g. insoluble corrosion products). The reasons related to the poor behaviors of 1 mmol/100ml imidazole on copper and brass can be various. On the basis of the figure 2.12, 2.13 and 2.14, both MBI and 1H-HB-2T have two different kinds of donor atoms (nitrogen atom and sulfur atom), while imidazole only has one kind of donor atom (nitrogen atom), so its simple structure may play a role because donor atoms can influence the chemisorption which is a key factor of the inhibition behavior of an organic inhibitor, as stated in the Chapter 1.3.

Then, the polarization resistances and the inhibition efficiencies of 1 mmol/100ml MBI and 1H-HB-2T were compared. Although inhibition efficiencies of MBI and 1H-HB-2T were different on different specimens, they were in a similar scale (higher than 92%) and changed with time. Therefore, it is difficult to make a conclusion on which one behaved better on copper and brass when the concentration was 1 mmol/100ml.

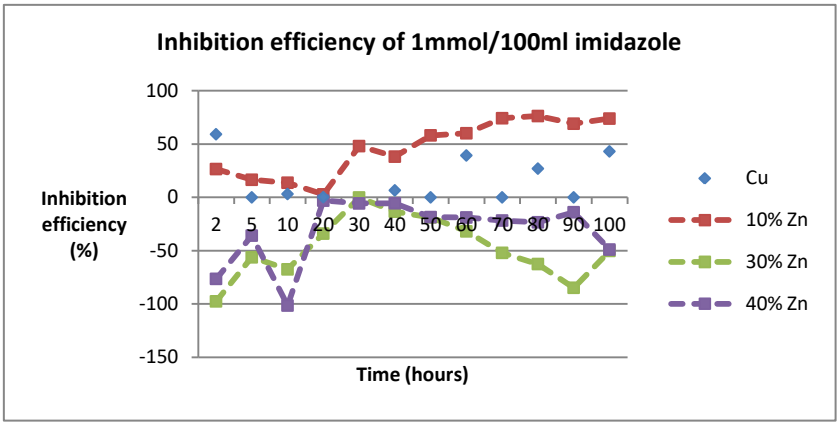

(a)

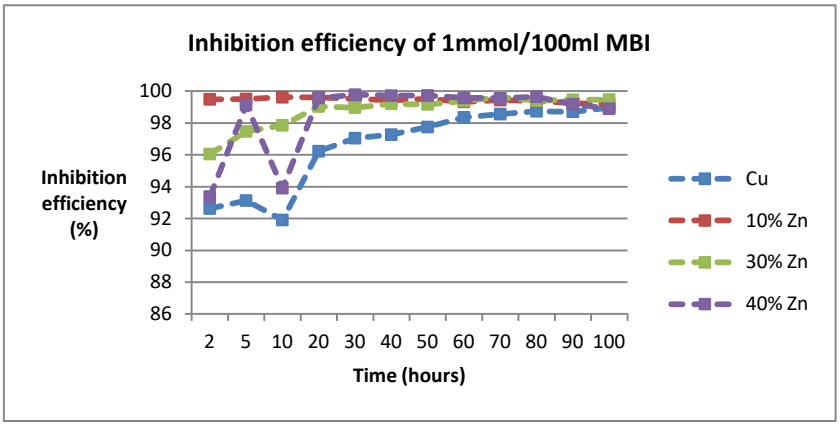

(b)

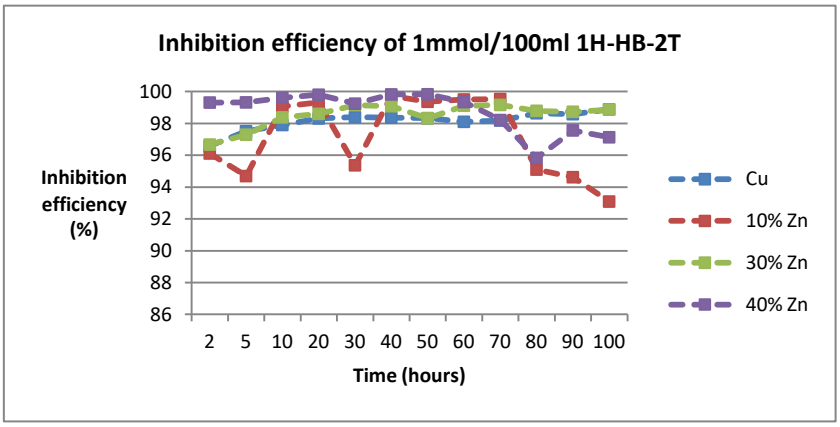

(c)

Figure 3.2 Inhibition efficiencies of 1 mmol/100ml (a) imidazole, (b) MBI, (c) 1H-HB-2T

Overall, 1 mmol/100ml imidazole was not an ideal corrosion inhibitor on tested materials compared with MBI and 1H-HB-2T with the same concentration, while MBI and 1H-HB-2T had similar inhibitions on copper and brass, so both MBI and 1H-HB-2T were chosen for the second stage of detailed analysis on their interaction mechanism.

According to the figure 3.1 (b) and (c), the polarization resistances of specimens immersed in the chosen organic inhibitors increased initially during the 100-hour-measurement. However, this increasing trend switched to an opposite trend after few hours of exposure. Afterwards, polarization resistances increased again and underwent a fluctuation. The change of the polarization resistances of immersed specimens was linked with an electrochemical process happened in the chloride aqueous solution. This electrochemical process contained both anodic and cathodic paths which took place at the surface of specimens (at the anodic area and the cathodic area, respectively). Attention was mainly paid to the anodic path of this electrochemical process, in which metal dissolution happened companying with an increasing potential. For copper and copper alloys, this process can be summarized by the following equations[29]:

$$Cu + Cl^- \rightarrow CuCl_{ads} + e^- \quad \text{eq. 3.1}$$

$$CuCl_{ads} + Cl^- \rightarrow CuCl_2{}^- \quad \text{eq. 3.2}$$

where $CuCl_{ads}$ was an adsorbed species at the specimen/solution interface.

The adsorbed species $CuCl_{ads}$ indicated the fact that in the anodic path, copper was adsorbed before taking part in the interfacial interaction with the molecules of inhibitors. During this interaction, thousands of interfacial bonds could be formed by electrostatic force (physisorption) or charge transfer (chemisorption). So for exposed copper and copper alloys, a mono-layer could be produced to cover their surface and protect them from corrosion. In this way, their polarization resistances would keep increasing in the early measuring time resulting in their promoted anti-corrosion ability.

Nevertheless, because of the corrosive solution (3wt% NaCl aqueous solution in this master thesis), these interfacial bonds at the specimen/solution interface could break after few hours resulting in several bare spots on the mono-layer. In this way, part of the surface of copper and copper alloys was exposed to the solvable aggressive species in the environment directly, so their polarization resistances went down and they became more susceptive to corrosion.

After corrosion happened, one or more kinds of stable corrosion products were produced and covered these bare spots where corrosion happened. This film of corrosion products could also provide effective protection against corrosive media. At the same time, broken interfacial bonds resulted from corrosive species in the environment could also be re-formed and re-protect the tested materials again. Under the synergistic effects of interfacial bonds and corrosion products, the polarization resistances of copper and brass went up again.

Because of the circulating process mentioned above, a fluctuation of the polarization resistances of copper and copper-zinc alloys collected by LPR measurement was

exhibited in the stage of inhibitors pre-selection.

3.2 Investigation on the inhibition mechanisms

This stage of detailed investigation on the interaction mechanisms of the chosen organic inhibitors on copper and brass was done by means of EIS and FTIR measurements. In EIS, valuable information is given by both Nyquist plot and Bode plot, an equivalent circuit is established for understanding physical meanings of each element of the tested corrosion system. In FTIR spectroscopy, since the energies required to vibrate is different for different functional groups, one single functional group shows a specific wavenumber or a range of wavenumbers in the FTIR spectrum as its significant characteristic. The data collected by FTIR spectroscopy are shown in the FTIR spectrum in which the wavenumber is the X-axis and intensity is the Y-axis.

As mentioned above that 1 mmol/100ml 2-mercapto-benzimidazole (MBI) and 2-mercapto-1-methyl-benzimidazole (1H-HB-2T) were chosen as the tested inhibitors in this stage of analysis, while pure copper, 50% Zn copper alloy (this composition ratio is a rough volume ratio as mentioned in the Chapter 2.5.2) and pure zinc thin film made by PVD were specimens.

3.2.1 Investigation on the adsorption

Ex-situ FTIR spectroscopy was employed to provide valuable information of the adsorption (chemisorption or physisorption) of the chosen organic inhibitors on the surface of specimens. In order to avoid the influence of aggressive species on the absorption and interfacial bonds, the chosen inhibitors were dissolved in MQ-water, rather than 3wt% NaCl aqueous solution, to prepare aqueous solution with concentration of 1 mmol/100ml.

In order to get information of functional groups of one organic inhibitor, it was measured by ex-situ FTIR spectroscopy before being dissolved in MQ-water. In this way, an ex-situ FTIR spectrum of this inhibitor was collected and showed various functional groups. Then, an ex-situ FTIR spectrum of one dried specimen which had immersed in 1 mmol/100ml inhibitor aqueous solution for 30 min was collected. By comparing these two ex-situ FTIR spectra, the functional groups of this organic inhibitor which contributed to the formation of interfacial bonds with the specimen surface could be found and the adsorption type of this inhibitor on the specimen could be defined.

What should be noticed is that in the ex-situ FTIR spectrum, two near peaks (both

positive or negative) appeared at the wavenumber around 2350 cm^{-1} were produced by the adsorption of carbon dioxide (CO_2) in the instrument, while continuous noises near 1300 to 2000 cm^{-1} and 3400 to 4000 cm^{-1} were caused by the adsorption of water vapor (H_2O)[30]. These noises can appear in both in-situ and ex-situ FTIR spectroscopy. In in-situ FTIR spectroscopy, they can be avoided by waiting for the added liquid nitrogen to vaporize and occupy the inside space of the instrument (it may take a long time). But in ex-situ FTIR spectroscopy, these noises cannot be avoided easily because of the mode used.

At the same time, because the spectral ranges of different modes used for ex-situ FTIR spectroscopy were different which have been discussed in detail in the Chapter 2.4.2, attention in this stage of investigation on the adsorption was only paid to the wavenumber range between 650 and 4000 cm^{-1}.

3.2.1.1 Adsorption of 1 mmol/100ml MBI

The ex-situ FTIR spectrum of 1 mmol/100ml MBI aqueous solution is shown in the figure 3.3. For MBI, functional groups mainly produced obvious peaks in the range from 900 to 1550 cm^{-1}. While for every specimen (pure copper, 50% Zn copper alloy and pure zinc) which had exposed to 1 mmol/100ml MBI for 30 min, a broad peak also appeared in this range. This broad peak was linked with an overlap of peaks related to MBI functional groups. Therefore, the existence of various MBI functional groups on the surface of specimens could be proved. In other word, electrostatic interaction between the whole molecule of MBI and specimens rather than a charge transfer between a specific MBI functional group and donor atoms happened.

Overall, the adsorption type of 1 mmol/100ml on copper, 50% Zn copper alloy and zinc was physisorption fulfilled by electrostatic force.

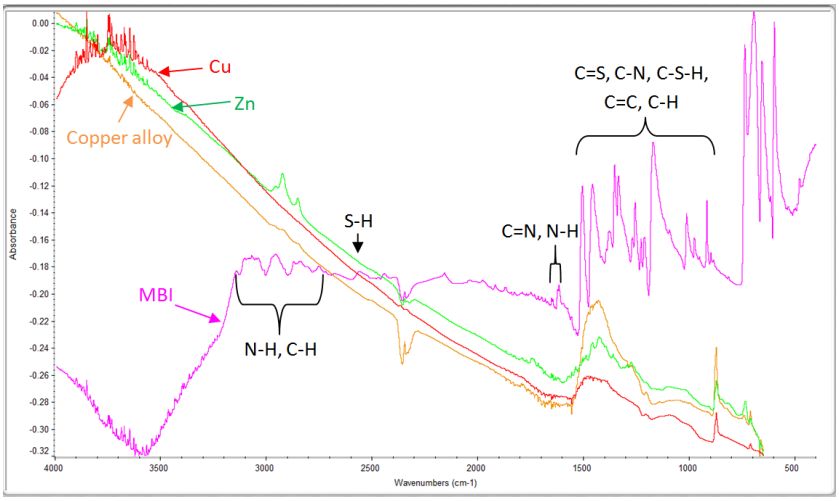

Figure 3.3 The ex-situ FTIR spectrum of 1 mmol/100ml MBI

3.2.1.2 Adsorption of 1 mmol/100ml 1H-HB-2T

The ex-situ FTIR spectrum of 1 mmol/100ml 1H-HB-2T aqueous solution is shown in the figure 3.4. In the target spectral range between 650 and 4000 cm^{-1}, peaks produced by functional groups of 1H-HB-2T mainly appeared in the range from 800 to 1550 cm^{-1}. A broad peak also appeared in this region for every tested material (pure copper, 50% Zn copper alloy and pure zinc) which had immersed in 1H-Hb-2T solution for half an hour. Similarly, this broad peak was linked with an overlap of peaks produced by different 1H-HB-2T functional groups, so electrostatic force between the whole molecule of 1H-HB-2T and specimens could be proved to play a more important role than the charge transfer between a specific MBI functional group and donor atoms during the adsorption process of 1H-HB-2T on copper, 50% Zn copper alloy and zinc.

Overall, the absorption type of 1 mmol/100ml 1H-Hb-2T on tested specimens was physisorption.

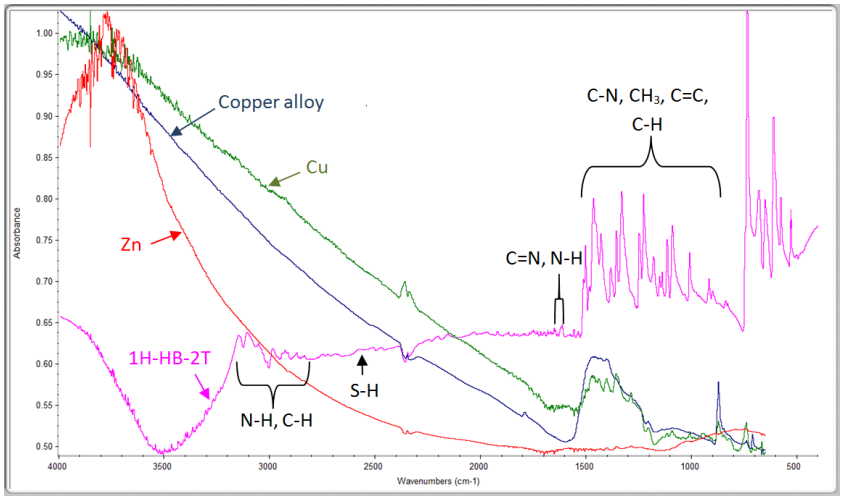

Figure 3.4 The ex-situ FTIR spectrum of 1 mmol/100ml 1H-HB-2T

3.2.2 Investigation on the interfacial interactions

In this stage of analysis, the chosen inhibitors (MBI and 1H-HB-2T) were dissolved in 3wt% NaCl aqueous solution to prepare 1 mmol/100ml solution. In order to understand the interfacial interactions between specimens and organic inhibitors, in-situ FTIR spectroscopy was used to collect quantitative and qualitative information. The in-situ FTIR spectrum which could show information collected by in-situ FTIR spectroscopy was baseline-corrected initially for distinguishing peaks of each functional group easily. However, the baseline-corrected in-situ FTIR spectrum should not be used for collecting the peak intensity of one peak.

In this stage of investigation of the interfacial interaction, since the intensity of liquid water was seen as constant during the immersion, the relative peak intensity

($\frac{\text{peak intensity of a functional group}}{\text{peak intensity of liquid water}}$) of peaks produced by various functional groups of organic inhibitors and its change with time were important. During in-situ FTIR spectroscopy, the peak intensity of air was used as the reference peak intensity or the background.

According to the figure 3.1 (b) and (c), the immersion times required for the polarization resistance of specimens to decrease were different, but generally, it was less than 20 hours. So the measuring time in this stage of analysis by means of EIS and in-situ FTIR measurements was set as 30 hours. In this way, the formation and the degradation of interfacial bonds between the surface of specimens and the molecules of inhibitors could be detected and recorded.

3.2.2.1 1 mmol/100ml MBI on pure copper thin film

The baseline-corrected in-situ FTIR spectrum of 1 mmol/100ml MBI on pure copper thin film deposited on the Ge crystal is shown in the figure 3.5. According to the structure shown in the figure 2.13, MBI has two different tautomeric forms. So its functional groups are possibly C-N, C=N, C-S and S-H (or C-S-H), C=S, C=C and C-H in aromatic. Peaks correspond to these functional groups are signed in the figure 3.5 and the change of their relative peak intensities in 30 hours collected from the non baseline-corrected in-situ FTIR spectrum is shown in the figure 3.6.

In the figure 3.5, C=N stretching vibration caused a peak at the wavenumber around 1648 cm^{-1}, compared with the peaks appeared at 1500 cm^{-1} produced by C=C stretching vibration and 739 cm^{-1} produced by C-S stretching vibration[31]. According to Hosseieni, Shanrabi and Nichols[32], the peak appeared at 1296 cm^{-1} was associated with a mutual effect of C-H bending, C-N stretching vibration and C-S-H deformation. On the basis of the Table of Infrared Spectroscopy Absorptions by Frequency Regions, the peak appeared at around 1352 cm^{-1} was associated with C-N stretching vibration, while that appeared at 1225 and 1275 cm^{-1} were linked with C=S and C-N stretching vibration, respectively.

In the figure 3.6, it is obvious that the relative peak intensities of peaks produced by MBI functional groups increased to their maximum values after 5 hours. Afterwards, they underwent a decrease. On the one hand, this trend reflected that MBI functional groups appeared on the copper thin film surface increased in the first 2 to 10 hours, then, a decrease happened. There is no doubt that this initial increase was caused by the formation of interfacial bonds between the copper thin film and the MBI molecules, while the decrease after 2 to 10 hours was caused by the break of these interfacial bonds. Since interfacial bonds contributed to the inhibition behavior of MBI, the inhibition effect of MBI on copper was best between 2 to 10 hours before the break of interfacial bonds happened. While when interfacial bonds began to break,

the inhibition of MBI would decrease. On the other hand, the trends of the relative peak intensity of each MBI functional group in 30 hours were similar, so the MBI molecule was proved again to be physisorbed on the copper film surface. Therefore, the short time required for interfacial bonds to break (2 to 10 hours) could be explained by the weak electrostatic interaction of physisorption.

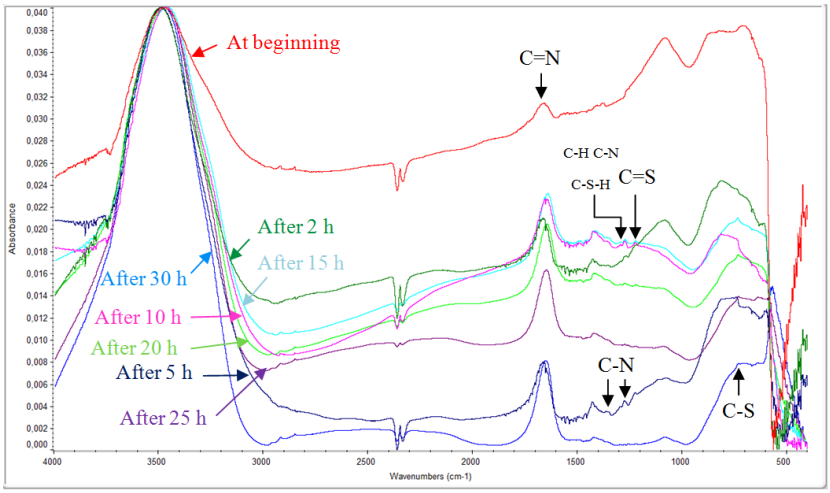

Figure 3.5 The baseline-corrected FTIR spectrum of 1 mmol/100ml MBI on pure copper thin film deposited on the Ge crystal in 30 hours

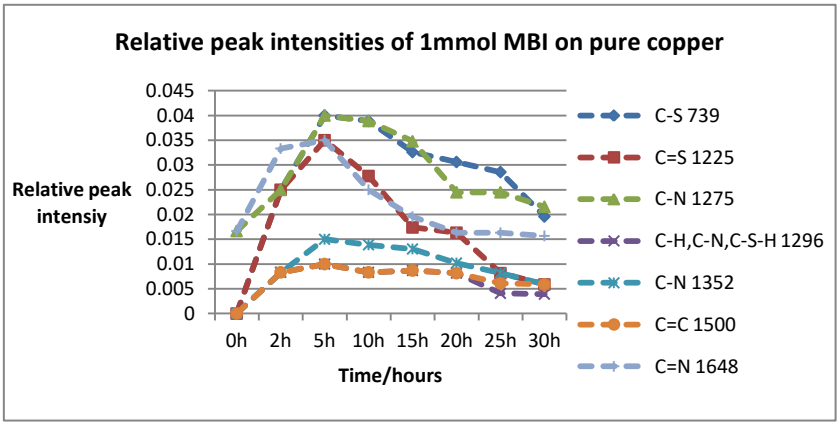

Figure 3.6 The relative peak intensities of MBI functional groups on pure copper thin film deposited on the Ge crystal in 30 hours

Similar information could also be collected from EIS. Nyquist plot and Bode plot are shown in the figure 3.7. In Nyquist plot, the radius of the semi-circle increased in the first 5 hours and arrived at its maximum value after 5 hours of immersion. Afterwards, the radius went through a decrease. According to the Chapter 2.3.1, the impedance at high frequency (on the left side of the X-axis) is equal to the ohmic resistance ($|Z| = R_\Omega$) which reflects the properties of solution and can be seen as unchanged during immersion, while that at low frequency (on the right side of the X-axis) is equal to the sum of the polarization resistance and the ohmic resistances ($|Z| = R_\Omega + R_P$). Therefore, the polarization resistance of copper immersed in 1 mmol/100ml MBI

increased in the first 2 to 10 hours. Although similar trend was not clear in Bode plot, it could be proved by an equivalent circuit established based on Nyquist plot and Bode plot. The equivalent circuit and corresponding impedance data are attached in the Appendix B. Therefore, when the immersion time was between 2 and 10 hours, copper owned the best anti-corrosion ability.

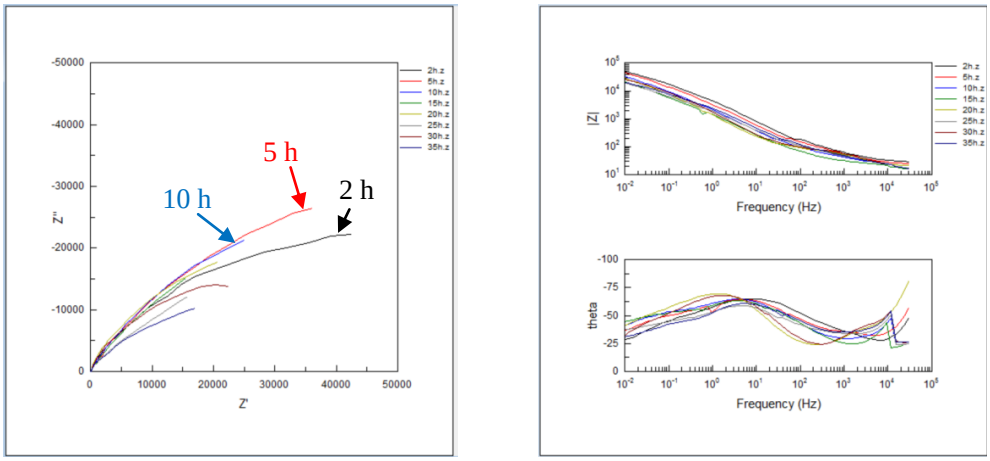

Figure 3.7 Nyquist (left) plot and Bode (right) plot of 1 mmol/100ml MBI on pure copper thin film deposited on the Ge crystal in 30 hours

In order to provide more comprehensive information of the inhibition effect of 1 mmol/100ml MBI on copper, the polarization resistances of copper collected by LPR measurement once every hour from 5 hours of immersion to 35 hours were plotted in the figure 3.8. According to this figure, the first peak of copper polarization resistance appeared after 7 hours. It can fit what got from in-situ FTIR and EIS measurements that when the immersion time was between 2 and 10 hours, the corrosion protection provided by 1 mmol/100ml MBI on copper was best and copper corrosion resistance was highest.

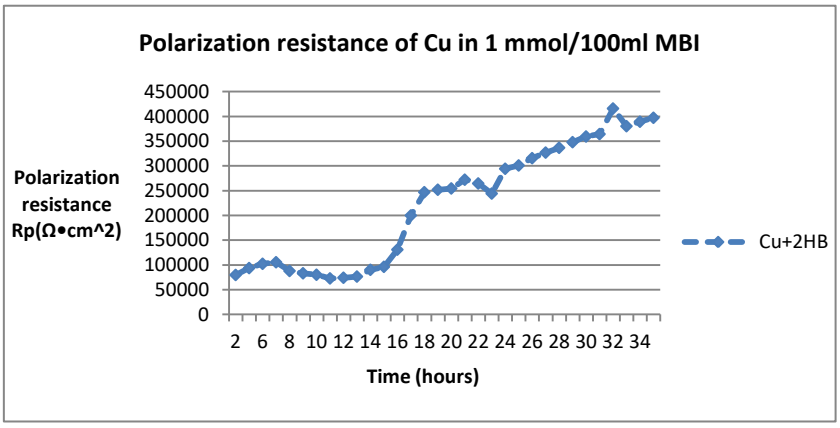

Figure 3.8 Polarization resistance of copper in 1 mmol/100ml MBI in 35 hours

Combing the figure 3.6 and 3.8, when the immersion time was longer than 2 to 10 hours, the trends of the relative peak intensities of various peaks and the polarization

resistance of copper were different (kept decreasing and increased again after a short-time decrease, respectively). The reason of this difference might be linked with the corrosion protection provided by insoluble corrosion products, because these corrosion products could also cover the bare copper surface and form a protective layer to resist or prevent corrosion. In other words, although MBI molecules were desorbed and interfacial bonds which could provide corrosion protection were broken, the protective layer of corrosion products on the copper surface could also enhance the anti-corrosion ability of copper.

Overall, it is rational to make a conclusion that 1 mmol/100ml MBI could provide complete corrosion protection on pure copper and this effect could last for around 2 to 10 hours. Afterwards, because of the corrosive environment (3wt% NaCl aqueous solution in this master thesis), interfacial bonds formed between MBI molecules and copper surface by electrostatic force would break, so the inhibition effect of MBI became weak and part of copper surface was exposed to the aggressive media directly.

3.2.2.2 1 mmol/100ml MBI on 50% Zn copper alloy thin film

The baseline-corrected in-situ FTIR spectrum of 1 mmol/100ml MBI on 50% Zn copper alloy thin film is shown in the figure 3.9, while the change of the relative peak intensities of peaks produced by MBI functional groups in 30 hours is shown in the figure 3.10.

Similar as discussed in the Chapter 3.2.2.1, C=N stretching vibration produced a peak at the wavenumber of around 1693 cm^{-1}, compared with the peak at 1483 cm^{-1} which was produced by C=C stretching vibration[31] . While the peak appeared at 1284 cm^{-1} was associated with a mutual effect of C-H bending, C-N stretching vibration and C-S-H deformation[32]. On the other hand, based on the Table of Infrared Spectroscopy Absorptions by Frequency Regions, the peaks appeared at around 1396 and 1363 cm^{-1} were linked with C-H bending and C-N stretching vibration, and peaks appeared at 1049 and 1612 cm^{-1} were produced by C=S and N-H bending vibration, respectively. These peaks are signed in the figure 3.9.

According to the figure 3.10, the relative peak intensities of peaks related to above functional groups all increased in the first 15 hours of exposure and arrived at their maximum values after 15 hours. Afterwards, a decrease happened. This trend indicated that MBI functional groups appeared on the alloy surface increased in the first 10 to 20 hours because of the formation of interfacial bonds at the specimen/solution interface. These bonds were formed by electrostatic force as concluded in the Chapter 3.2.1.1. Combined with the corrosion protection mechanism of organic inhibitors, the inhibition effect of 1 mmol/100ml MBI on 50% Zn copper alloy was strengthened in the first 10 to 20 hours. However, when MBI functional groups on the alloy surface began to decrease because of the break of interfacial

bonds, the inhibition effect of MBI on the alloy began to be weaker.

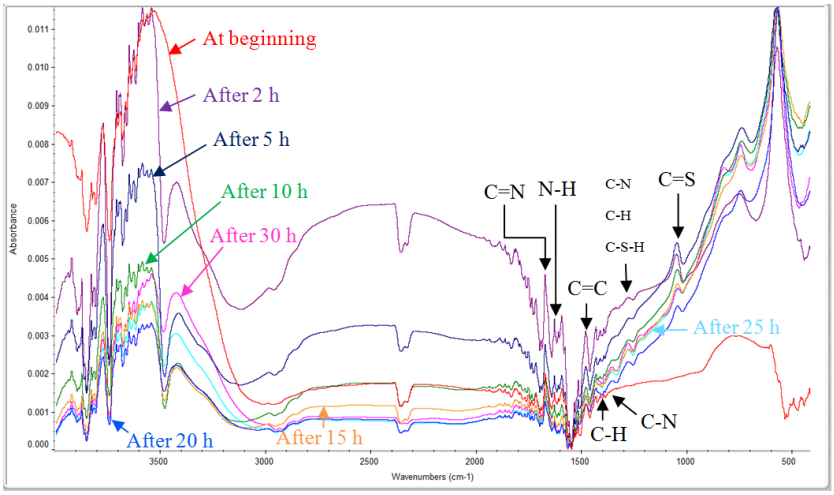

Figure 3.9 The baseline-corrected FTIR spectrum of 1 mmol/100ml MBI on 50% Zn copper alloy thin film deposited on the Ge crystal in 30 hours

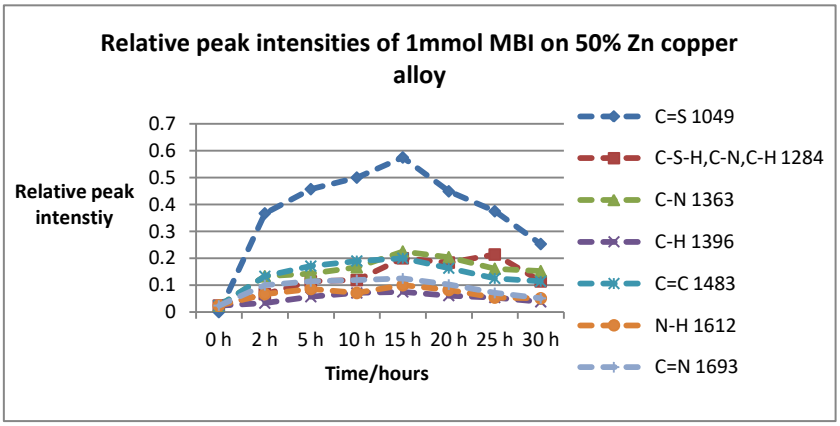

Figure 3.10 The relative peak intensities of functional groups of MBI on 50% Zn copper alloy thin film deposited on the Ge crystal in 30 hours

EIS could confirm results got from in-situ FTIR spectroscopy. Nyquist plot and Bode plot are shown in the figure 3.11. Since curves in Bode plot were too dense, especially at the low frequency region, more attention was paid to Nyquist plot. Similarly, combining the Chapter 2.3.1 and the radius of the semi-circle in Nyquist plot, the polarization resistance of 50% Zn copper alloy increased in the first 15 hours when it was immersed in the 1 mmol/100ml MBI solution. Afterwards, it decreased smoothly. The equivalent circuit established based on both Nyquist plot and Bode plot could also provide the same trend of the polarization resistance of the alloy. The fitted equivalent circuit and corresponding impedance data are attached in the Appendix C. The polarization resistance trend could reflect the change of the corrosion resistance of exposed 50 % Zn copper alloy in 30 hours (increased in the first 10 to 20 hours and decreased afterwards).

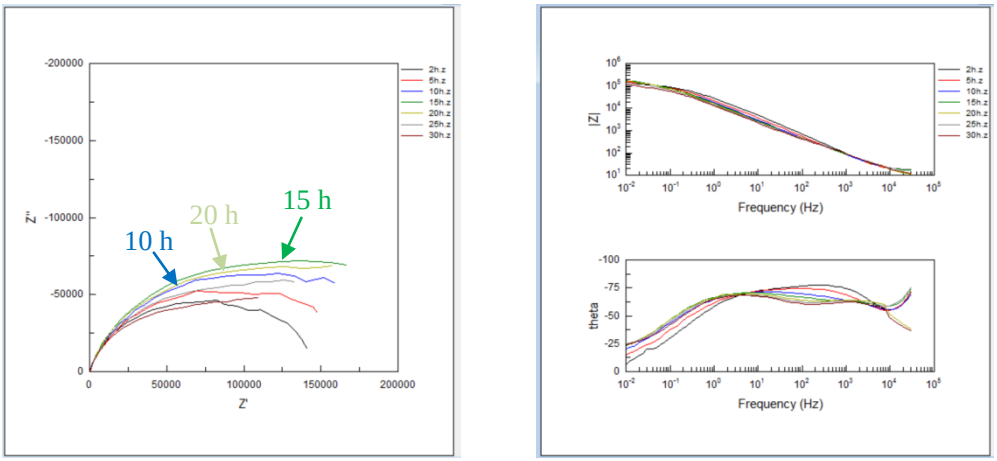

Figure 3.11 Nyquist (left) plot and Bode (right) plot of 1 mmol/100ml MBI on 50% Zn copper alloy thin film deposited on the Ge crystal in 30 hours

Overall, a conclusion can be made that 1 mmol/100ml MBI could provide complete corrosion protection on 50% Zn copper alloy when the immersion time was less than 10 to 20 hours. But the inhibition effect of MBI began to be weak after 10 to 20 hours because of the break of interfacial bonds at the specimen/solution interface, so the anti-corrosion ability of the copper alloy became weak.

3.2.2.3 1 mmol/100ml MBI on pure zinc thin film

Figure 3.12 shows the baseline-corrected FTIR spectrum of 1 mmol/100ml MBI on pure zinc thin film deposited on the Ge crystal. Figure 3.13 expresses the change of the relative peak intensities of peaks produced by MBI functional groups in 30 hours.

For MBI, C=N stretching vibration caused a peak at the wavenumber of around 1656 cm^{-1}, compared with peaks at 1500 and 605 cm^{-1} which were associated with C=C and C-S stretching vibration, respectively[31]. Meantime, the peak appeared at 1649 cm^{-1} was linked with a mutual effect of N-H and C-H bending vibration based on the study of Hosseieni, Shanrabi and Nichols[32]. Another mutual effect happened at the wavenumber of 1296 cm^{-1}, which combined C-H bending, C-N stretching vibration and C-S-H deformation[32]. On the basis of the Table of Infrared Spectroscopy Absorptions by Frequency Regions, the peak appeared at around 1277 cm^{-1} was associated with C-N stretching vibration, while that appeared at 1225 cm^{-1} was linked with C=S stretching vibration. These peaks are all signed in the figure 3.12.

In the figure 3.13, the relative peak intensities of peaks linked with MBI functional groups all arrived at their first peak after 2 hours of exposure. Afterwards, they decreased and underwent a fluctuation, then arrived at another peak after around 15 hours. These two peaks reflected that when the exposure time were within 5 hours as well as between 10 and 20 hours, MBI functional groups appeared on the zinc film surface arrived at their peak values. The increase of MBI functional groups on the

zinc was fulfilled by the formation of interfacial bonds between the zinc surface and MBI molecules, while the decreases happened after the peak values were caused by the break of those interfacial bonds. Based on the protection mechanism of organic inhibitors, the inhibition effect of 1 mmol/100ml MBI on zinc was best when the immersion time were within 5 hours as well as between 10 and 20 hours.

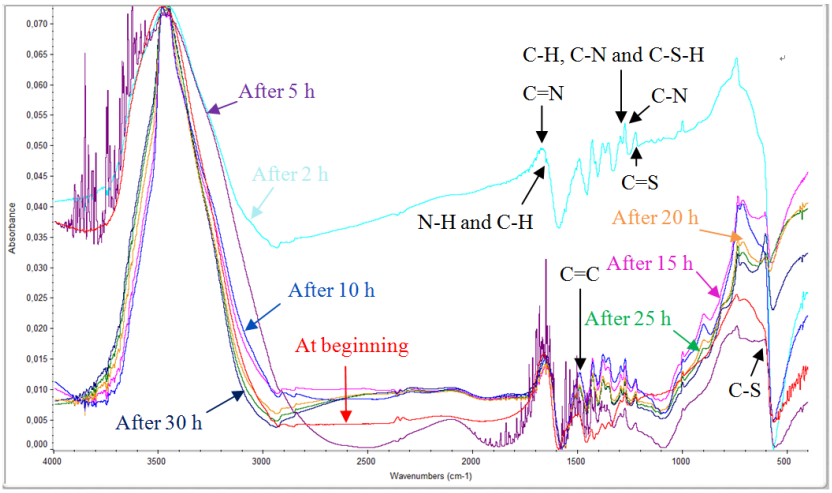

Figure 3.12 The baseline-corrected FTIR spectrum of 1 mmol/100ml MBI on pure zinc film deposited on the Ge crystal in 30 hours

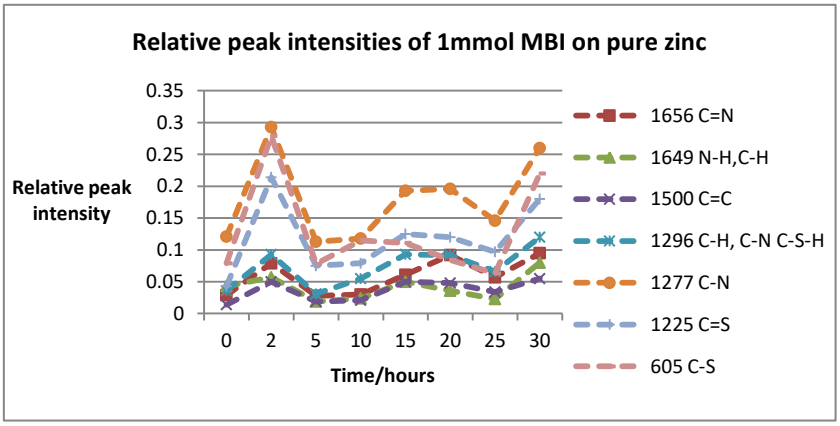

Figure 3.13 The relative peak intensities of functional groups of MBI on pure zinc film deposited on the Ge crystal in 30 hours

Figure 3.14 shows Nyquist plot and Bode plot recorded by EIS. In both Nyquist plot and Bode plot, the curve measured after 2 hours was totally different from others. Since it is a normal phenomenon for EIS that the measurement is unstable and inaccurate in the early measuring time, curves measured after 2 hours in Nyquist plot and Bode plot cannot be persuasive enough to give any useful information. Since curves in Bode plot were too dense, especially at the low frequency region, attention was mainly paid to Nyquist plot. In Nyquist plot, when the relative peak intensities of peaks produced by MBI functional groups reached their second peak value, i.e. when the immersion time was 15 hours, the radius of the semi-circle increased to its

maximum value. Namely, the polarization resistance of zinc immersed in 1 mmol/100ml MBI reached its maximum value after 10 to 20 hours. This trend could be further proved by an equivalent circuit and corresponding impedance data attached in the Appendix D. Therefore, anti-corrosion ability of zinc was best when the immersion time was between 10 and 20 hours.

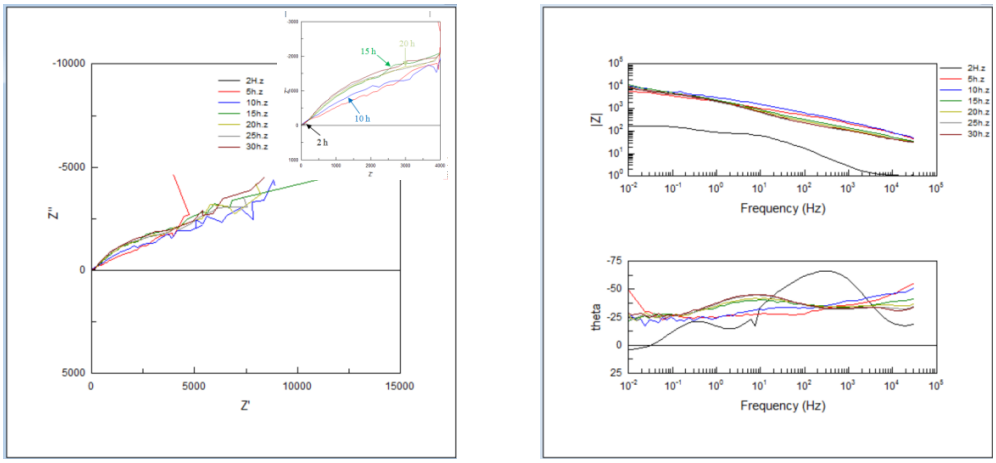

Figure 3.14 Nyquist (left) plot and Bode (right) plot of 1 mmol/100ml MBI on pure zinc thin film deposited on the Ge crystal in 30 hours

In order to obtain more comprehensive information of the inhibition effect of 1 mmol/100ml MBI on zinc, outcomes got from in-situ FTIR and EIS measurements were compared with a detailed trend of zinc polarization resistance collected by LPR measurement once every hour from 5 hours of immersion to 35 hours. This detailed trend is shown in the figure 3.15. In this figure, the polarization resistance of exposed zinc only had one obvious peak which appeared after 9 hours.

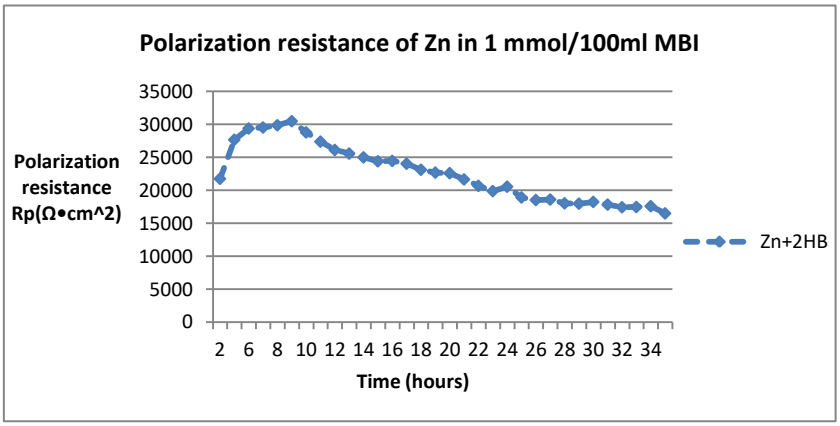

Figure 3.15 Polarization resistance of zinc in 1 mmol/100ml MBI in 35 hours

Combing the figure 3.13, 3.14 and 3.15, different information was given by in-situ FTIR, EIS and LPR measurements. In in-situ FTIR spectroscopy, the best adsorption status of MBI on the zinc surface happened after 2 hours and 15 hours of immersion, it meant that best inhibition effect of 1 mmol/100ml MBI on zinc appeared within 5

hours and after 10 to 20 hours. In EIS, because of the instability in the early measuring time, the peak value of zinc polarization resistance (collected from Nyquist plot and the equivalent circuit) and the best anti-corrosion behavior of immersed zinc arose after 10 to 20 hours. So EIS could fit in-situ FTIR spectroscopy. In LPR measurement, however, the polarization resistance of the immersed zinc was highest when the immersion time was 9 hours.

One of the possible reasons linked with the difference mentioned above could be the different surface conditions. In in-situ FTIR and EIS measurements which were performed at the same time, because of the requirement of direct contact between the ATR crystal and the specimen on the basis of the Kretschmann geometry, zinc was deposited by PVD on the Ge crystal with a thickness of around 13.3 nm. Hence, the zinc thin film had a mirror like surface. Nevertheless, the zinc sheets used in LPR measurement were polished mechanically with different grades of silicon carbide paper (from 320 to 4000).

Another reason may be the fact that one organic corrosion inhibitor can behave differently on different specimens. It could be reflected by the figure 3.1 and 3.2. Furthermore, according to Zarrouk[33], the inhibition behavior of an inhibitor not only depends on its structure (e.g. the number of donor atoms, the molecular size and the charge density), but also depends on the mode of adsorption, the formation of metallic complexes, the characteristic of the environments, the nature of the metal surface and so on. Although the inhibition effects of 1 mmol/100ml MBI on pure copper and copper-zinc alloys were perfect, MBI might not be an ideal and suitable inhibitor on pure zinc which was exposed to 3wt% NaCl aqueous solution. Hence, the addition of MBI might not reduce the corrosion rate of zinc dramatically although its adsorption on the zinc surface could also happen.

Because of the poor inhibition effect of 1 mmol/100ml MBI on zinc, corrosion happened and a protective layer of corrosion products (possible be ZnO, $Zn(OH)_2$ or $Zn_5(OH)_8Cl_2 \cdot 2H_2O$) was produced and covered on the zinc surface[34]. This layer of corrosion products was thought as the major mechanism to provide corrosion protection and affect the polarization resistance of zinc.

3.2.2.4 1 mmol/100ml 1H-HB-2T on pure copper thin film

The baseline-corrected in-situ FTIR spectrum of 1 mmol/100ml 1H-HB-2T on pure copper thin film deposited on the Ge crystal is shown in the figure 3.16. According to the structure of 1H-HB-2T shown in the figure 2.14, its functional groups are C-N, C=N, S-H, C-S, CH_3, C=C and C-H in aromatic. Since peaks of S-H (in the wavenumber region from 2550 to 2600 cm^{-1}) and C-S (in the wavenumber region from 570 to 710 cm^{-1}) were too weak, it is difficult to distinguish them and measure their peak intensities in the FTIR spectrum. At present, limited studies have done on

in-situ FTIR spectroscopy of 1H-HB-2T, so the Table of Infrared Spectroscopy Absorptions by Frequency Regions played an important role in the analysis of 1H-HB-2T on specimens. From the Table of Infrared Spectroscopy Absorptions by Frequency Regions, the peak appeared at around 2833 cm^{-1} was associated with C-H stretching vibration, while that appeared at 1656 cm^{-1} was linked with C=N stretching vibration. Meantime, C=C stretching vibration was indicated by the peak at 1502 cm^{-1}. CH_3 vibration and C-N stretching vibration produced two peaks at about 1375 cm^{-1} and 1339 cm^{-1}, respectively. These peaks are signed in the figure 3.16. The change of the relative peak intensities of peaks linked with above functional groups is shown in the figure 3.17.

According to the figure 3.17, the relative peak intensities all underwent an increase initially and arrived at their maximum values after around 10 hours. Afterwards, a smooth decline happened. On the one hand, this trend indicated that 1H-HB-2T functional groups appeared on the copper surface increased in the first 5 to 15 hours, then, they decreased. Therefore, it is reasonable to define that interfacial bonds formed initially between the immersed copper surface and 1H-HB-2T molecules. After 5 to 15 hours, these bonds broke because of the corrosive environment. On the other hand, the trend of the relative peak intensities of various peaks produced by 1H-HB-2T functional groups in 30 hours were similar, so the occurrence of physisorption of the whole 1H-HB-2T molecule on the copper surface could be proved. At the same time, the short time required for interfacial bonds to break (between 5 to 15 hours) could be explained by the weak electrostatic force and low energy of physisorption.

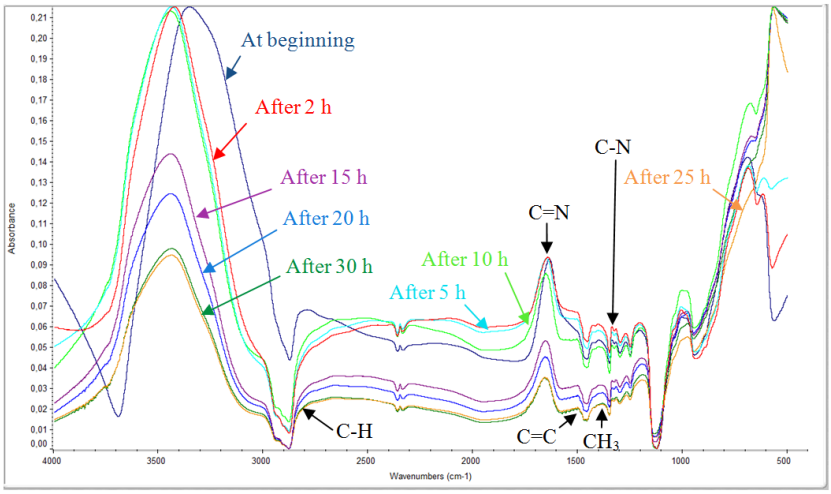

Figure 3.16 The baseline-corrected FTIR spectrum of 1 mmol/100ml 1H-HB-2T on pure copper film deposited on the Ge crystal in 30 hours

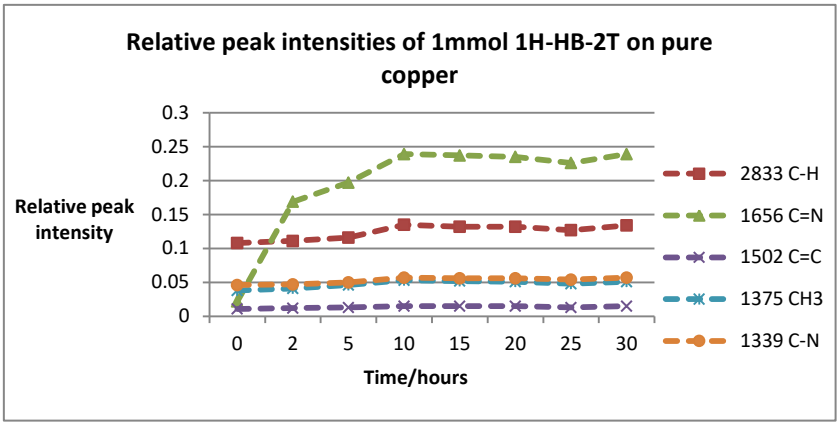

Figure 3.17 The relative peak intensities of functional groups of 1H-HB-2T on pure copper film deposited on the Ge crystal in 30 hours

Similar information can be collected from EIS. Nyquist plot and Bode plot of 1 mmol/100ml 1H-HB-2T on pure copper thin film are shown in the figure 3.18. Since curves in Bode plot were too dense, especially at the low frequency region, useful information cannot be collected from Bode plot. In Nyquist plot, however, valuable information can be collected. Combining the increasing radius of the semi-circle in Nyquist plot and the Chapter 2.3.1, the polarization resistance of copper increased in the first 5 to 15 hours and its anti-corrosion ability was enhanced at the same time. When the immersion time was longer, the radius decreased smoothly and the anti-corrosion ability of copper began to be weak, so copper began to become more susceptive to corrosion. Same as the trend of the relative peak intensities shown in the figure 3.17, the trend of the radius of the semi-circle (or the polarization resistance of immersed copper) became opposite after 25 hours of immersion. The tendency of the copper polarization resistance could also be proved by an equivalent circuit established based on Nyquist plot and Bode plot. The equivalent circuit and corresponding impedance data are attached in the Appendix E.

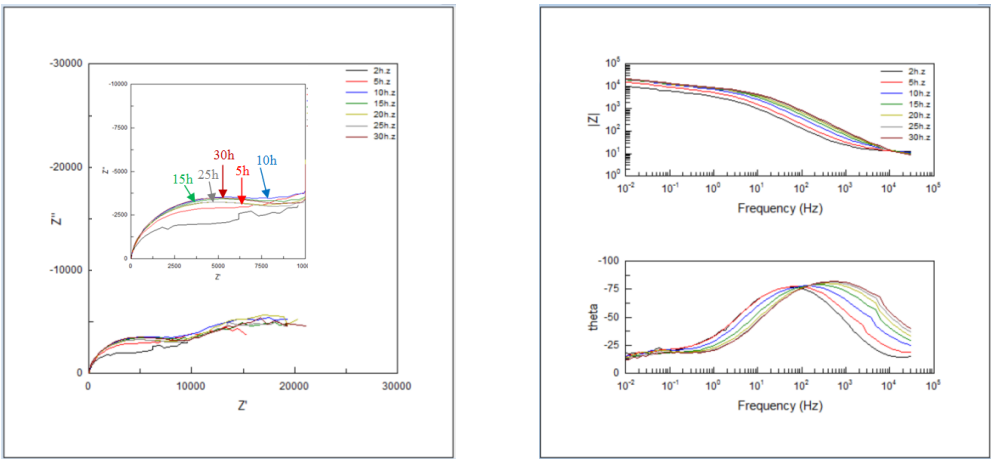

Figure 3.18 Nyquist (left) plot and Bode (right) plot of 1 mmol/100ml 1H-HB-2T on pure copper thin film deposited on the Ge crystal in 30 hours

Similarly, a detailed change of the polarization resistance of exposed copper was plotted in the figure 3.19 in order to provide more comprehensive information of the inhibition effect of 1 mmol/100ml 1H-HB-2T on copper. In the figure 3.19, a peak value appeared after 12 hours. It can fit what got from in-situ FTIR and EIS measurements that when the immersion time was 5 to 15 hours, the corrosion protection provided by 1H-HB-2T on copper was the best and the corrosion resistance of copper was the highest.

Similar as discussed in the Chapter 3.2.2.1 that the change of the relative peak intensities shown in the figure 3.17 and the polarization resistance of copper shown in the figure 3.19 were different after their peak (underwent a fluctuation and kept increasing, respectively). The reason of this difference may be a protective layer formed by corrosion products on the copper surface. In other words, although the physisorption of MBI molecules onto the copper surface became weak after few hours, corrosion could be resisted by a protective layer of corrosion products.

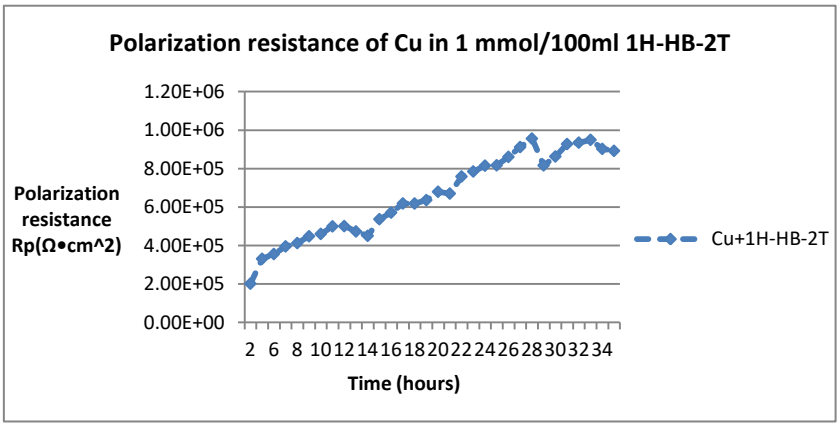

Figure 3.19 Polarization resistance of copper in 1 mmol/100ml 1H-HB-2T in 35 hours

Overall, a conclusion can be made that 1 mmol/100ml 1H-HB-2T could provide corrosion protection on pure copper in 3wt% NaCl solution and the physisorption of 1H-HB-2T was strengthened in the early measuring time, so its inhibition effect became better initially. But after 5 to 15 hours, because of the corrosive species in the solution, break of interfacial bonds at the specimen/solution interface which contributed to the corrosion protection of 1H-HB-2T happened resulting in its weakened inhibition effect.

3.2.2.5 1 mmol/100ml 1H-HB-2T on 50% Zn copper alloy thin film

The figure 3.20 indicates the baseline-corrected FTIR spectrum of 1 mmol/100ml 1H-HB-2T on 50% Zn copper alloy thin film. Since peaks of S-H in the wavenumber region from 2550 to 2600 cm^{-1} were too weak and the existence of noises caused by the instrument in the wavenumber region from 570 to 710 cm^{-1}, S-H and C-S could

not be distinguished from the in-situ FTIR spectrum. According to the Table of Infrared Spectroscopy Absorptions by Frequency Regions, the peak appeared at around 1676 cm^{-1} was linked with C=N stretching vibration, while that appeared at 1452 cm^{-1} was associated with CH_3 deformation. Meantime, C-N stretching vibration produced a series of peaks in the region between 1230 and 1360 cm^{-1}, C-H bending vibration produced two peaks at about 825 cm^{-1} and 748 cm^{-1}. These peaks are signed in the figure 3.20. The change of the relative peak intensities of peaks produced by them measured from the non-baseline-corrected FTIR spectrum is shown in the figure 3.21.

In the figure 3.21, the relative peak intensities of peaks produced by 1H-HB-2T functional groups arrived at their maximum values after 10 hours of immersion. Then, there was a fluctuation. It meant that 1H-HB-2T molecules adsorbed on the alloy surface increased in the first 5 to 15 hours and decreased afterwards. This increase was fulfilled by the formation of interfacial bonds at the specimen/solution interface under electrostatic force, while the decrease was linked with the break of those interfacial bonds. Since the adsorption of one organic inhibitor and the formation of interfacial bonds play a significant role in the inhibition effect of this inhibitor, it is reasonable to inference that the inhibition effect of 1 mmol/100ml 1H-HB-2T on 50% Zn copper alloy was enhanced initially and was best when the immersion time was between 5 and 15 hours, then in the following few hours, it became weak because of the break of interfacial bonds.

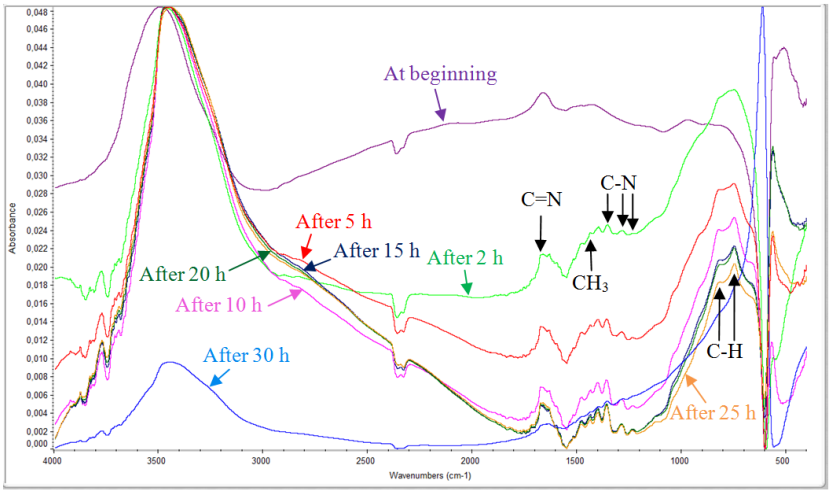

Figure 3.20 The baseline-corrected FTIR spectrum of 1 mmol/100ml 1H-HB-2T on 50% Zn copper alloy film deposited on the Ge crystal in 30 hours

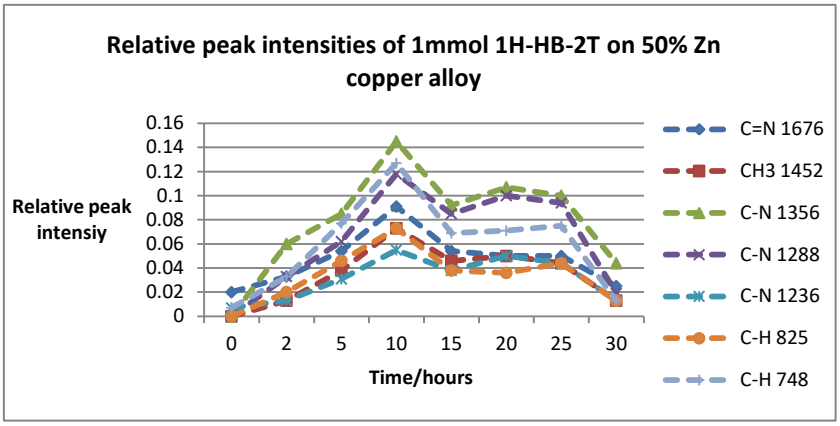

Figure 3.21 The relative peak intensities of functional groups of 1H-HB-2T on 50% Zn copper alloy film deposited on the Ge crystal in 30 hours

Same information of the inhibition behavior of 1 mmol/100ml 1H-HB-2T on 50% Zn copper alloy could also be reflected by Nyquist plot and Bode plot shown in the figure 3.22. Based on the change of the semi-circle radius in Nyquist plot, the increasing impedance at low frequency began to decrease after 10 hours. Therefore, the increasing polarization resistance of the 50% Zn copper alloy underwent a decrease after 5 to 15 hours. Similar trend could also be seen in Bode plot, in which the curve collected after 10 hours was higher than others at the low frequency. As mentioned in the Chapter 2.3.1 that the impedance at the low frequency region in Bode plot is equal to the sum of the ohmic resistance and the polarization resistance ($|Z| = R_\Omega + R_P$). Since the ohmic resistance is seen as unchanged during the measurement, the polarization resistance of the alloy was highest when the immersion time was 5 to 15 hours. Information got from Nyquist plot and Bode plot could be further proved by an equivalent circuit and corresponding impedance data attached in the Appendix F. Therefore, when 50% Zn copper alloy was immersed in 1 mmol/100ml 1H-HB-2T, its corrosion resistance increased and became the highest after 5 to 15 hours. Afterwards, it began to decrease and the alloy began to be more sensitive to corrosion.

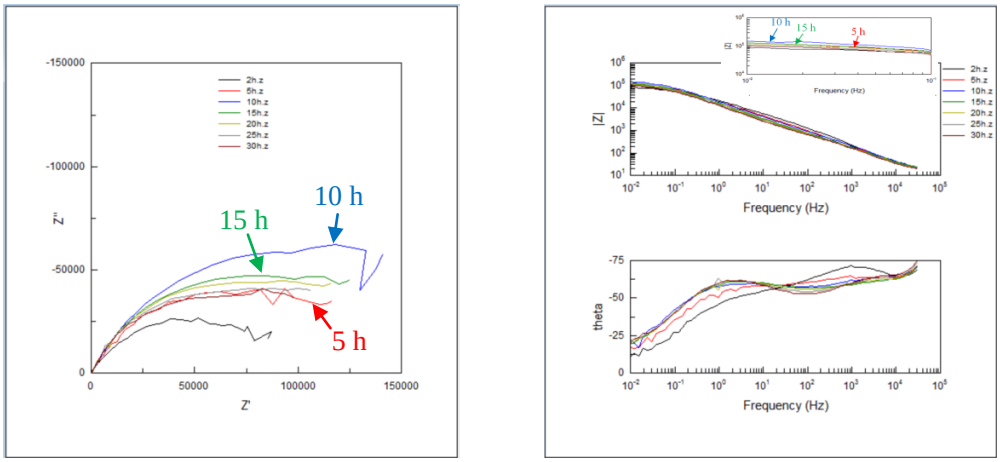

Figure 3.22 Nyquist (left) plot and Bode (right) plot of 1 mmol/100ml 1H-HB-2T on 50% Zn copper alloy thin film deposited on the Ge crystal in 30 hours

Overall, 1 mmol/100ml 1H-HB-2T could provide complete corrosion protection on 50% Zn copper alloy in 3 wt% NaCl solution within a certain exposure time. In the first 5 to 15 hours, the inhibition effect of 1H-HB-2T was strengthened, so the anti-corrosion ability of the alloy became better with time. Afterwards, however, because of the aggressive environment and the relative low adsorption energy of physisorption of 1H-HB-2T molecules, break of interfacial bonds happened. Hence, the inhibition effect of 1H-HB-2T dropped and the alloy became more susceptive to corrosion.

3.2.2.6 1 mmol/100ml 1H-HB-2T on pure zinc thin film

The baseline-corrected in-situ FTIR spectrum of 1 mmol/100ml 1H-HB-2T on pure zinc thin film is shown in the figure 3.23, while the change of the relative peak intensities of various peaks produced by 1H-HB-2T functional groups is shown in the figure 3.24.

Similarly, peaks of S-H and C-S were difficult to be distinguished from the FTIR spectrum, other peaks related to 1H-HB-2T functional groups were signed in the figure 3.23 on the basis of the Table of Infrared Spectroscopy Absorptions by Frequency Regions. The peak appeared at the wavenumber of around 2940 cm^{-1} was associated with C-H stretching vibration, that appeared at 1646 cm^{-1} was linked with C=N stretching vibration. Meantime, C=C stretching vibration was indicated by a peak at around 1480 cm^{-1}. CH_3 vibration and C-N stretching vibration produced two peaks at about 1452 cm^{-1} and 1257 cm^{-1}, respectively. Another peak linked with the C-H bending vibration appeared in the wavenumber region between 800 and 900 cm^{-1}.

In the figure 3.24, the maximum relative peak intensity of each peak appeared after 15 hours. It meant that 1H-HB-2T functional groups appeared on the zinc surface increased in the first 10 to 20 hours, but afterwards, they began to decrease. As stated in the former chapters that the increase of 1H-HB-2T molecules on the zinc surface was linked with the formation of interfacial bonds at the specimen/solution interface, while the later decrease was caused by the break of these bonds because of the aggressive agent. Based on the fact that interfacial bonds played a major role in the corrosion protection of 1H-HB-2T, a preliminary conclusion could be made that the inhibition effect of 1 mmol/100ml 1H-HB-2T on zinc was the best when the immersion time was between 10 and 20 hours, afterwards, it became weak.

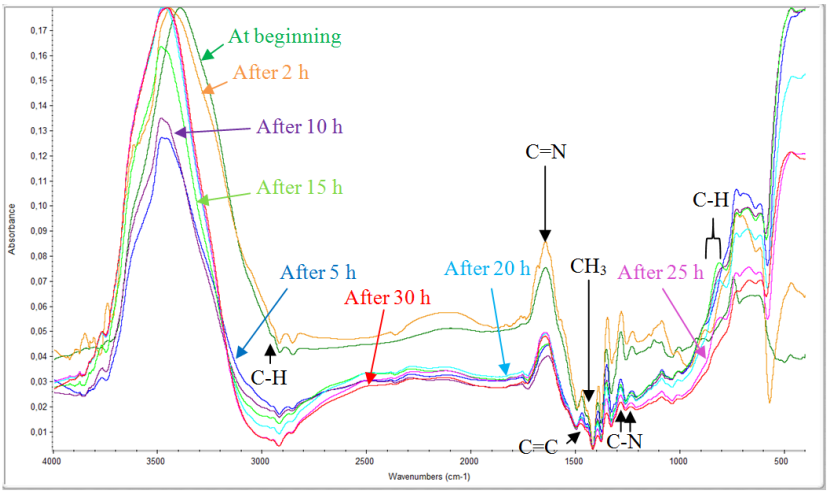

Figure 3.23 The baseline-corrected FTIR spectrum of 1 mmol/100ml 1H-HB-2T on pure zinc film deposited on the Ge crystal in 30 hours

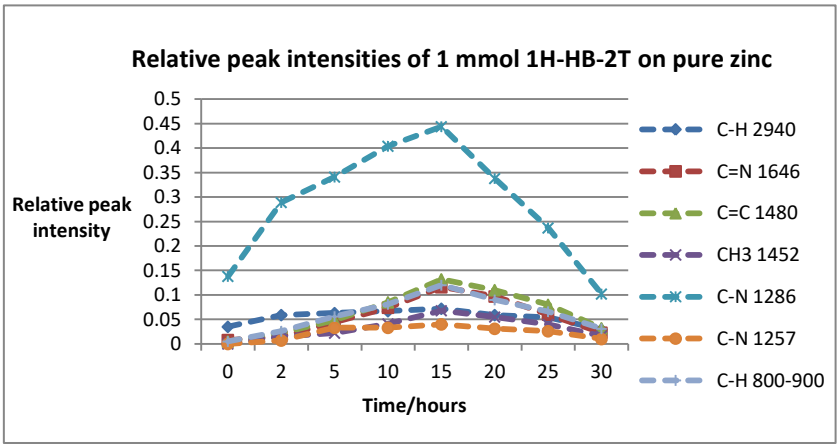

Figure 3.24 The relative peak intensities of functional groups of 1H-HB-2T on pure zinc film deposited on the Ge crystal in 30 hours

This preliminary conclusion got from in-situ FTIR spectroscopy could be proved by Nyquist plot and Bode plot collected by means of EIS. Nyquist plot and Bode plot are shown in the figure 3.25. The change of the radius of the semi-circle in Nyquist plot and the change of the impedance at the low frequency region in Bode plot reflected that the polarization resistance of zinc immersed in 1 mmol/100ml 1H-HB-2T increased and reached its maximum value when the immersion time was 10 to 20 hours. Afterwards, the trend became opposite. Similar trend was also indicated by an equivalent circuit set up based on both Nyquist plot and Bode plot. According to the equivalent circuit and corresponding impedance data shown in the Appendix G, the change of zinc polarization resistance in 30 hours collected by EIS could be plotted and proved the appearance of the highest zinc polarization resistance and the best anti-corrosion ability of zinc which happened after 10 to 20 hours.

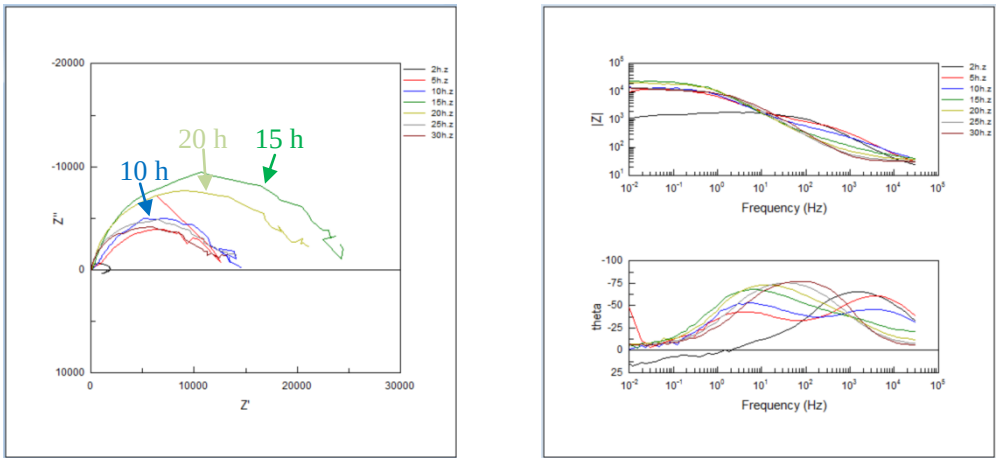

Figure 3.25 Nyquist (left) plot and Bode (right) plot of 1 mmol/100ml 1H-HB-2T on pure zinc thin film deposited on the Ge crystal in 30 hours

In order to further provide more comprehensive information of the inhibition effect of 1 mmol/100ml 1H-HB-2T on pure zinc, the polarization resistances of zinc collected by LPR measurement once every hour from 5 hours of immersion to 35 hours were plotted and exhibited in the figure 3.26. Compared with the results got from in-situ FTIR and EIS measurements, different information was give by this figure about the time required for zinc polarization resistance to arrive at its peak value (10 hours rather than between 10 and 20 hours).

Similarly as stated in the Chapter 3.2.2.3 that one of the possible reasons resulted in this difference may be the different surface conditions of specimens used in these measurements, i.e. mirror-like deposited surface in in-situ FTIR and EIS measurements versus surface prepared by silicon carbide paper in LPR measurement. Another possible reason linked with this difference was the poor inhibition effect of 1 mmol/100ml 1H-HB-2T on zinc. Although 1H-HB-2T worked well on copper and brass in 3 wt% NaCl aqueous solution, it might not be an effective inhibitor on pure zinc[33]. In other words, the addition of 1H-HB-2T might not reduce the corrosion rate of zinc dramatically although the electrostatic interaction existed between the zinc surface and 1H-HB-2T molecules. Hence, the anti-corrosion ability of the immersed zinc might mainly result from a layer of corrosion products (possible be ZnO, $Zn(OH)_2$ or $Zn_5(OH)_8Cl_2 \cdot 2H_2O$) on the zinc surface[34]. But according to the figure 3.26, in the first 35 hours, the zinc polarization resistance decreased after the peak value, so the corrosion protection provided by the layer of corrosion products might not work well initially because of the corrosive environment.

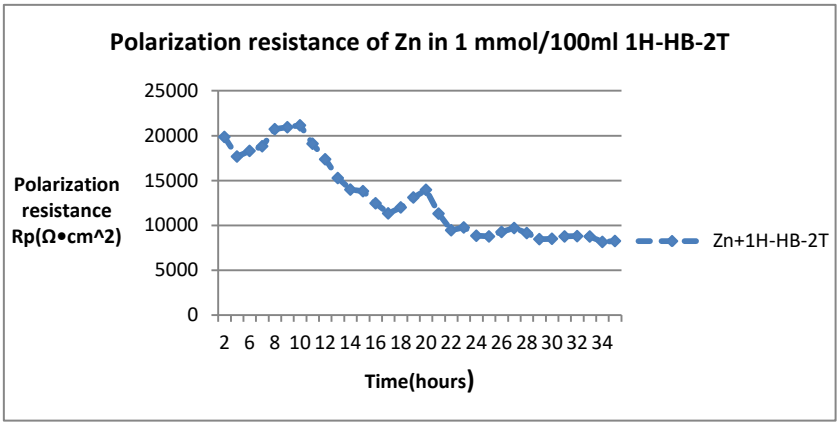

Figure 3.26 Polarization resistance of zinc in 1 mmol/100ml 1H-HB-2T in 35 hours

Overall, it is convincing to make a conclusion that the inhibition effect of 1 mmol/100ml 1H-HB-2T on pure zinc was not as well as that on copper and brass, although the physisorption behavior of its molecules also happened at the specimen/solution interface. Meantime, when the immersion time was between 10 to 20 hours, not protective mono-layer formed by interfacial bonds broke because of the aggressive environment (3wt% NaCl aqueous solution).

Chapter 4 CONCLUSIONS

Different organic corrosion inhibitors exhibit different inhibition behaviors on copper and brass because of the influence of structure, physicochemical and electronic properties of organic compounds and surfaces. Compared with 1 mmol/100ml 2-mercapto-benzimidazole (MBI) and 2-mercapto-1-methyl-benzimidazole (1H-HB-2T), imidazole with the same concentration shows a weak inhibition effect on copper and brass. On the other hand, one kind of organic corrosion inhibitor also behaved differently on different specimens. Inhibitions of 1 mmol/100ml MBI and 1H-HB-2T on copper and brass are high, but their inhibitions on zinc was much weaker than with copper.

The interaction mechanisms of 1 mmol/100ml MBI and 1H-HB-2T on copper and brass are linked with the electrostatic force between the molecules and the surface of specimens. During the physisorption process, interfacial bonds were formed at the specimen/solution interface and produced a protective mono-layer retarding corrosion. The aggressive electrolyte (3wt% NaCl aqueous solution) breaks the interfacial bond after few hours of immersion. Therefore, inhibition effects of MBI and 1H-HB-2T on specimens became weaker after a relatively similar exposure time. The time required for the interfacial bond to break depends on the inhibitor and specimen types.

APPENDIX A

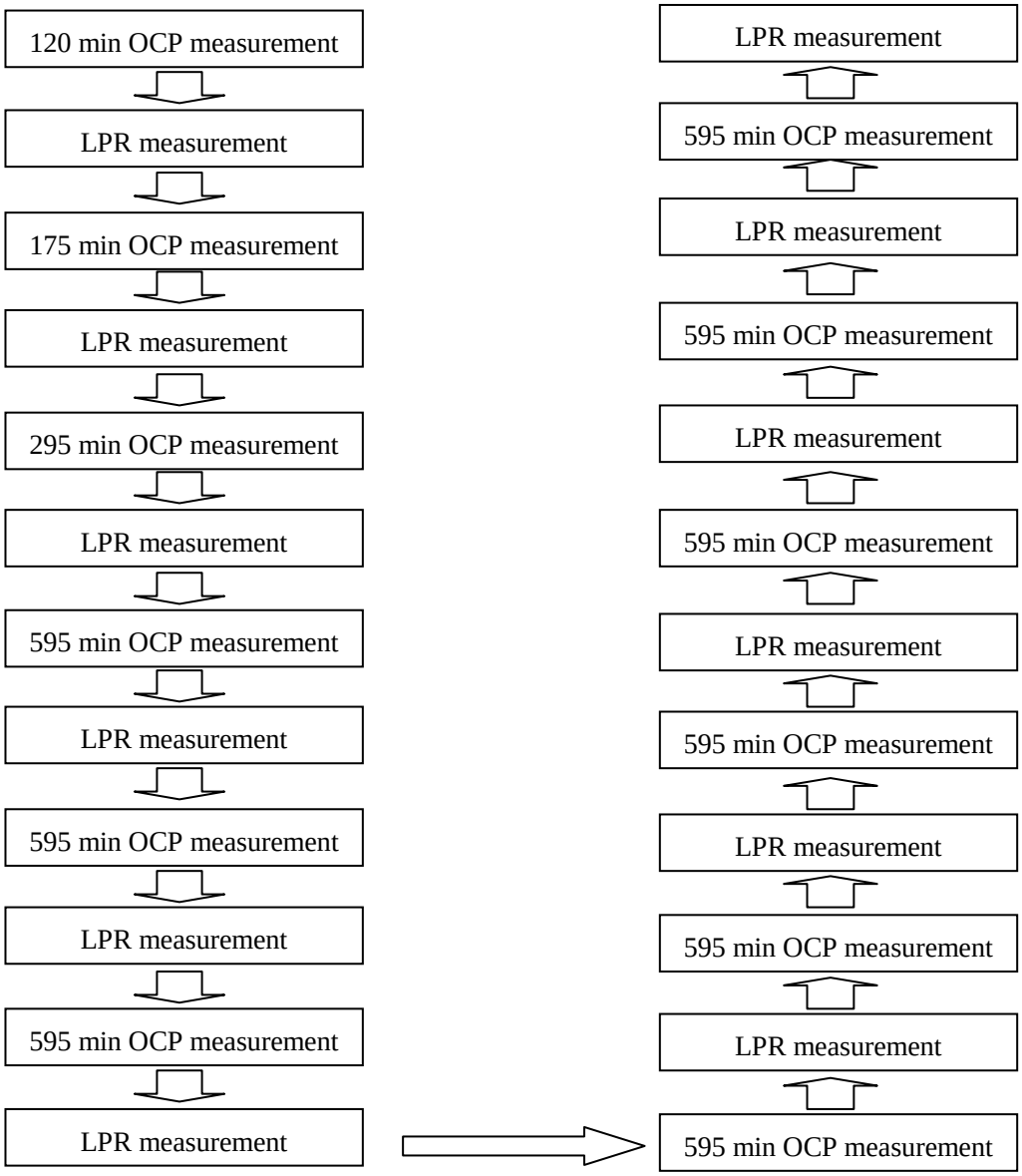

Table A-1 Experiment set of LPR measurement

APPENDIX B

1 mmol/100ml 2-mercapto-benzimidazole (MBI) on pure copper thin film

Figure B-1 The equivalent circuit

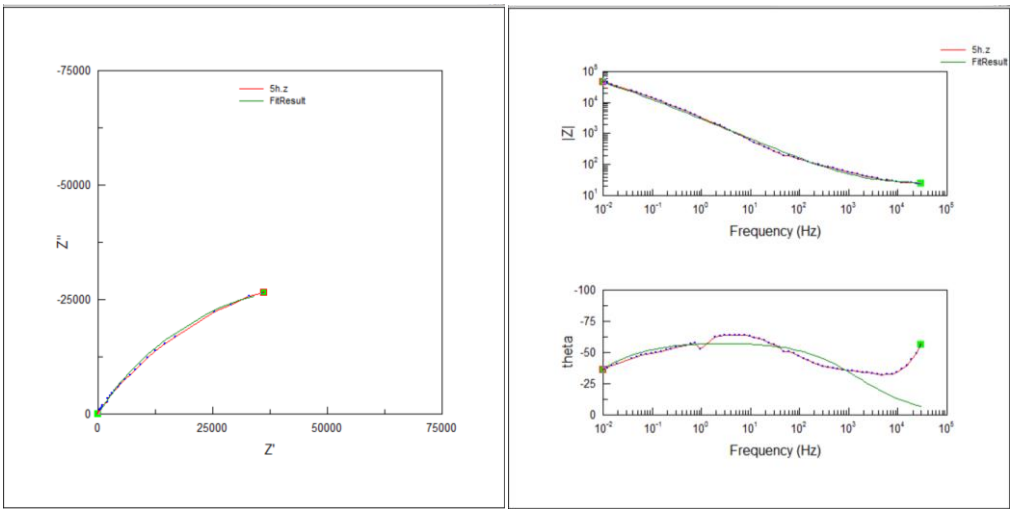

Figure B-2 The fitting plots

Table B-1 Impedance data after 2 hours of immersion

	Value	Error	Error%
R_s	27.83	1.3783	4.9526
C_{coat}-T	7.0705E-05	2.2757E-06	3.2186
C_{coat}-P	0.67741	0.006953	1.0264
R_p	66578	6011.2	9.0288

Table B-2 Impedance data after 5 hours of immersion

	Value	Error	Error%
R_s	24.14	1.6278	6.7432
C_{coat}-T	0.00010098	2.9975E-06	3.9587
C_{coat}-P	0.6524	0.008658	1.3271
R_p	99295	22247	22.405

Table B-3 Impedance data after 10 hours of immersion

	Value	Error	Error%
R_s	21.62	1.2106	5.5994
C_{coat}-T	0.00015337	5.494E-06	3.5822
C_{coat}-P	0.66167	0.0086359	1.3052
R_p	89946	27216	30.258

Table B-4 Impedance data after 15 hours of immersion

	Value	Error	Error%
R_s	19.19	0.8176	4.2606
C_{coat}-T	0.00023044	6.8893E-06	2.9896
C_{coat}-P	0.66074	0.0076009	1.1504
R_p	60015	12865	21.436

Table B-5 Impedance data after 20 hours of immersion

	Value	Error	Error%
R_s	39.42	3.2256	8.1826
C_{coat}-T	0.0002178	1.2722E-05	5.8411
C_{coat}-P	0.7136	0.018149	2.5433
R_p	57880	21653	37.41

Table B-6 Impedance data after 25 hours of immersion

	Value	Error	Error%
R_s	15.13	0.99049	6.5465
C_{coat}-T	0.00020539	6.3731E-06	3.1029
C_{coat}-P	0.57875	0.0067104	1.1595
R_p	60668	14485	23.876

Table B-7 Impedance data after 30 hours of immersion

	Value	Error	Error%
R_s	31.51	2.7082	8.5947
C_{coat}-T	0.00018132	9.8037E-06	5.4068
C_{coat}-P	0.67073	0.014994	2.2355
R_p	53960	16330	30.263

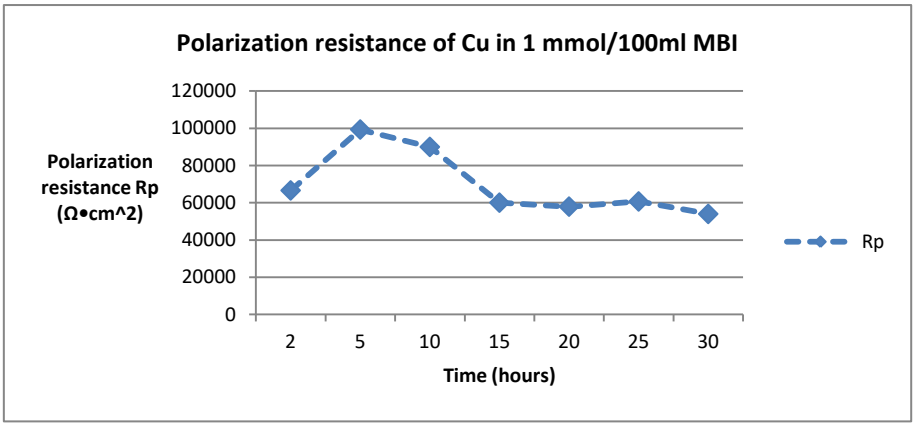

Figure B-3 The change of polarization resistance of Cu in 1 mmol/100ml MBI got from EIS

APPENDIX C

1 mmol/100ml 2-mercapto-benzimidazole (MBI) on 50% Zn copper alloy thin film

Figure C-1 The equivalent circuit

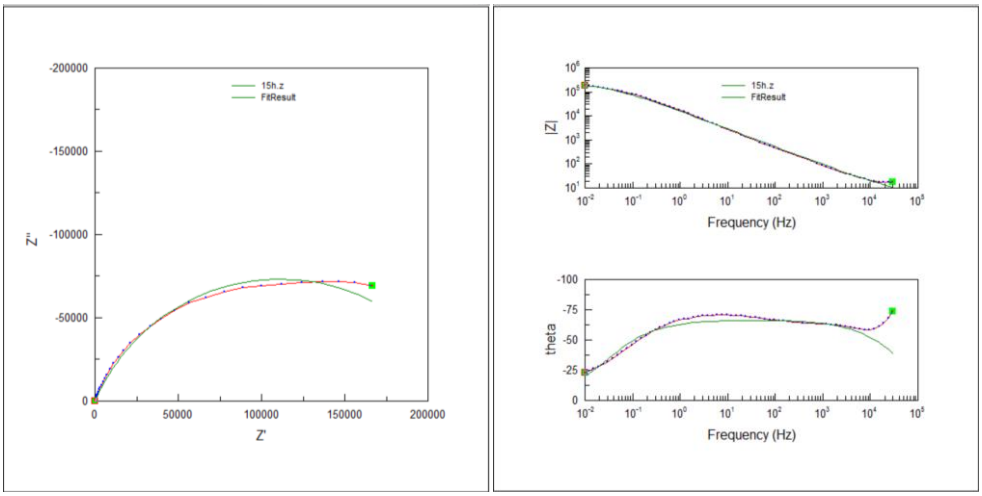

Figure C-2 The fitting plots

Table C-1 Impedance data after 2 hours of immersion

	Value	Error	Error%
R_s	7.279	0.83966	11.535
C_{coat}-T	7.8412E-06	2.9195E-07	3.7233
C_{coat}-P	0.80711	0.0058212	0.72124
R_p	130150	5260.2	4.0416

Table C-2 Impedance data after 5 hours of immersion

	Value	Error	Error%
R_s	7.638	0.85772	11.23
C_{coat}-T	1.1033E-05	3.8359E-07	3.4768
C_{coat}-P	0.7839	0.0056495	0.72069
R_p	152030	7342.3	4.8295

Table C-3 Impedance data after 10 hours of immersion

	Value	Error	Error%
R_s	7.262	0.78272	10.778
C_{coat}-T	1.4446E-05	4.2467E-07	2.9397
C_{coat}-P	0.75922	0.0048216	0.63507
R_p	188320	10322	5.4811

Table C-4 Impedance data after 15 hours of immersion

	Value	Error	Error%
R_s	5.558	0.8374	15.067
C_{coat}-T	1.6107E-05	4.8318E-07	2.9998
C_{coat}-P	0.74169	0.004837	0.65216
R_p	222290	15260	6.8649

Table C-5 Impedance data after 20 hours of immersion

	Value	Error	Error%
R_s	5.761	0.25439	4.4157
C_{coat}-T	1.5913E-05	1.8059E-07	1.1349
C_{coat}-P	0.75271	0.0017818	0.23672
R_p	205910	4854.4	2.3575

Table C-6 Impedance data after 25 hours of immersion

	Value	Error	Error%
R_s	4.202	0.8903	21.188
C_{coat}-T	1.9535E-05	5.9843E-07	3.0634
C_{coat}-P	0.71439	0.004855	0.6796
R_p	189230	14086	7.4439

Table C-7 Impedance data after 30 hours of immersion

	Value	Error	Error%
R_s	6.368	0.33283	5.2266
C_{coat}-T	2.0223E-05	2.8859E-07	1.427
C_{coat}-P	0.72949	0.00225043	0.30848
R_p	142570	4016.1	2.8169

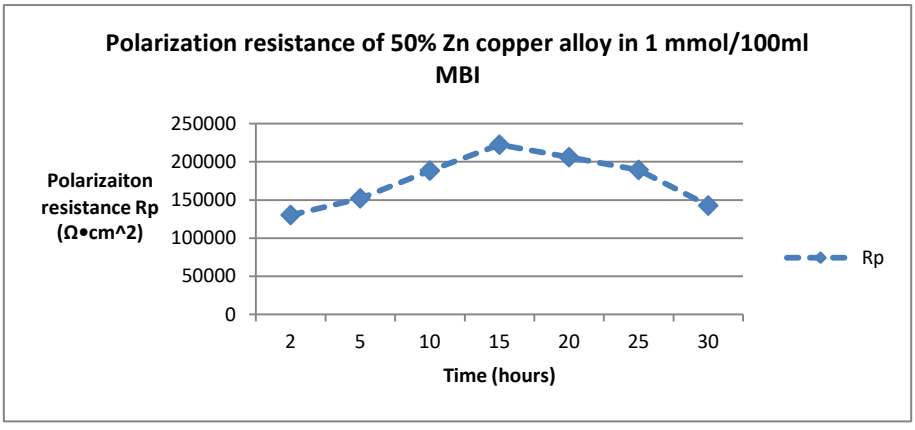

Figure C-3 The change of polarization resistance of 50% Zn copper alloy in 1 mmol/100ml MBI got from EIS

APPENDIX D

1 mmol/100ml 2-mercapto-benzimidazole (MBI) on pure zinc thin film

Figure D-1 The equivalent circuit

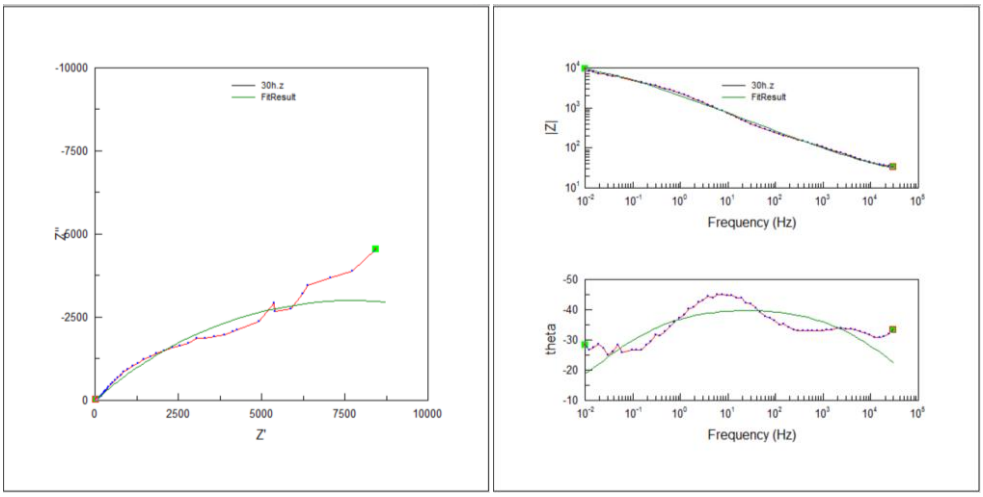

Figure D-2 The fitting plots

Table D-1 Impedance data after 2 hours of immersion

	Value	Error	Error%
R_s	0.79213	0.046022	5.8099
C_{coat}-T	0.00049665	4.4632E-05	8.9866
C_{coat}-P	0.7637	0.013041	1.7076
R_p	138.9	3.9424	2.8383

Table D-2 Impedance data after 5 hours of immersion

	Value	Error	Error%
R_s	0.96904	0.13377	7.2441
C_{coat}-T	0.00019044	1.0082E-05	5.2941
C_{coat}-P	0.36859	0.0069089	1.8744
R_p	9190	859.27	9.3501

Table D-3 Impedance data after 10 hours of immersion

	Value	Error	Error%
R_s	3.833	0.25396	0.66256
C_{coat}-T	0.00013076	2.7026E-06	2.0668
C_{coat}-P	0.37344	0.0033147	0.88761
R_p	16304	685.65	4.2054

Table D-4 Impedance data after 15 hours of immersion

	Value	Error	Error%
R_s	2.838	1.3491	47.537
C_{coat}-T	0.00018482	3.7105E-06	2.0076
C_{coat}-P	0.42187	0.0034033	0.80672
R_p	22421	1777.3	7.9269

Table D-5 Impedance data after 20 hours of immersion

	Value	Error	Error%
R_s	8.65	1.2135	14.029
C_{coat}-T	0.00019326	4.1069E-06	2.1251
C_{coat}-P	0.44242	0.0037008	0.83649
R_p	15714	880.36	5.6024

Table D-6 Impedance data after 25 hours of immersion

	Value	Error	Error%
R_s	14.49	1.4047	9.6943
C_{coat}-T	0.00020249	5.3865E-06	2.6601
C_{coat}-P	0.46127	0.0048272	1.0465
R_p	13545	858.67	6.3394

Table D-7 Impedance data after 30 hours of immersion

	Value	Error	Error%
R_s	15.58	1.3525	8.681
C_{coat}-T	0.0001899	4.8127E-06	2.5343
C_{coat}-P	0.46832	0.0046422	0.99125
R_p	15558	995.65	6.3996

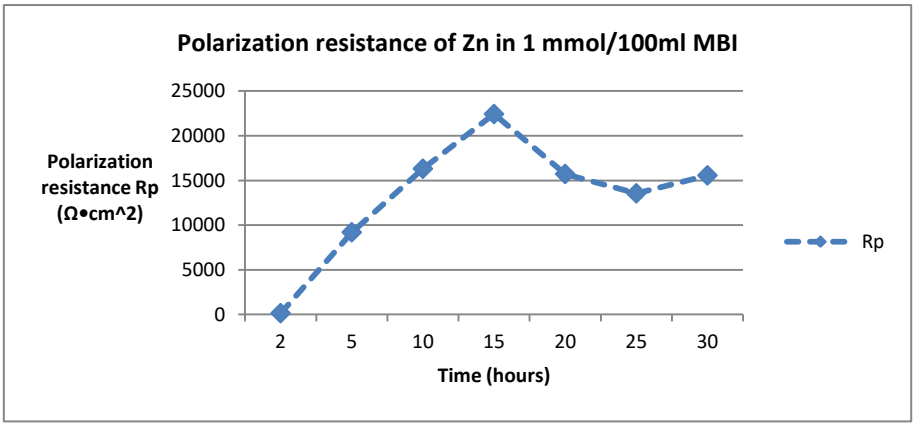

Figure D-3 The change of polarization resistance of Zn in 1 mmol/100ml MBI got from EIS

APPENDIX E

1 mmol/100ml 2-mercapto-1-methyl-benzimidazole (1H-HB-2T) on pure copper film

Figure E-1 The equivalent circuit

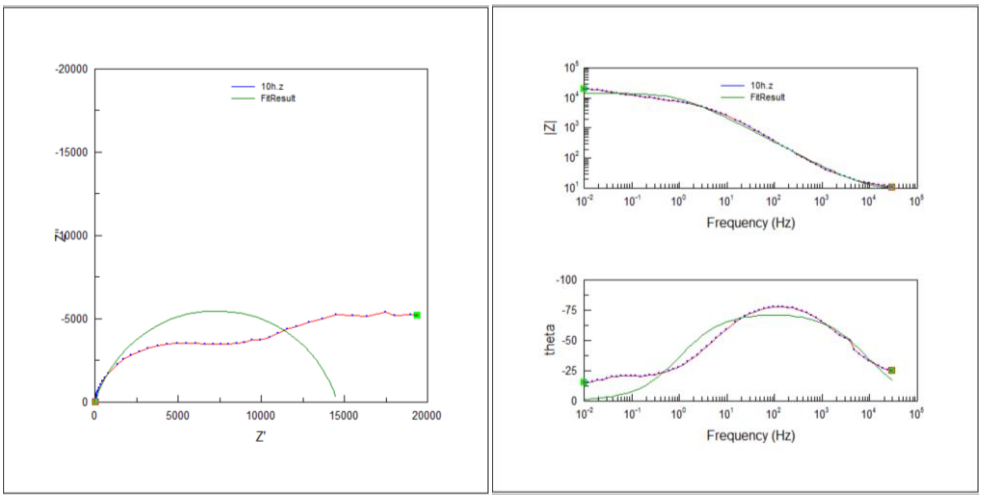

Figure E-2 The fitting plots

Table E-1 Impedance data after 2 hours of immersion

	Value	Error	Error%
R_s	11.15	0.49772	4.4639
C_{coat}-T	3.7078E-05	2.1787E-06	5.876
C_{coat}-P	0.82589	0.010075	1.2199
R_p	7590	253.49	3.3398

Table E-2 Impedance data after 5 hours of immersion

	Value	Error	Error%
R_s	10.4	0.54298	5.221
C_{coat}-T	2.4778E-05	1.4089E-06	5.6861
C_{coat}-P	0.82312	0.0093092	1.131
R_p	11634	392.68	3.3753

Table E-3 Impedance data after 10 hours of immersion

	Value	Error	Error%
R_s	8.894	0.64061	7.2027
C_{coat}-T	1.4835E-05	9.3131E-07	6.2778
C_{coat}-P	0.82068	0.0094769	11548
R_p	14569	506.67	3.4777

Table E-4 Impedance data after 15 hours of immersion

	Value	Error	Error%
R_s	7.451	0.66646	8.9446
C_{coat}-T	9.7968E-06	6.7149E-07	6.8542
C_{coat}-P	0.83368	0.0097673	1.1716
R_p	14059	472.15	3.3583

Table E-5 Impedance data after 20 hours of immersion

	Value	Error	Error%
R_s	6.102	0.75331	12.345
C_{coat}-T	7.8802E-06	6.4732E-07	8.2145
C_{coat}-P	0.84076	0.011337	1.3484
R_p	14046	530.79	3.7789

Table E-6 Impedance data after 25 hours of immersion

	Value	Error	Error%
R_s	5.418	0.73378	13.543
C_{coat}-T	6.3581E-06	5.2817E-07	8.307
C_{coat}-P	0.85301	0.011173	1.3098
R_p	13658	490.78	3.5934

Table E-7 Impedance data after 30 hours of immersion

	Value	Error	Error%
R_s	4.788	0.73703	15.393
C_{coat}-T	5.6129E-06	4.6671E-07	8.315
C_{coat}-P	0.85804	0.011043	1.287
R_p	14590	521.22	3.5724

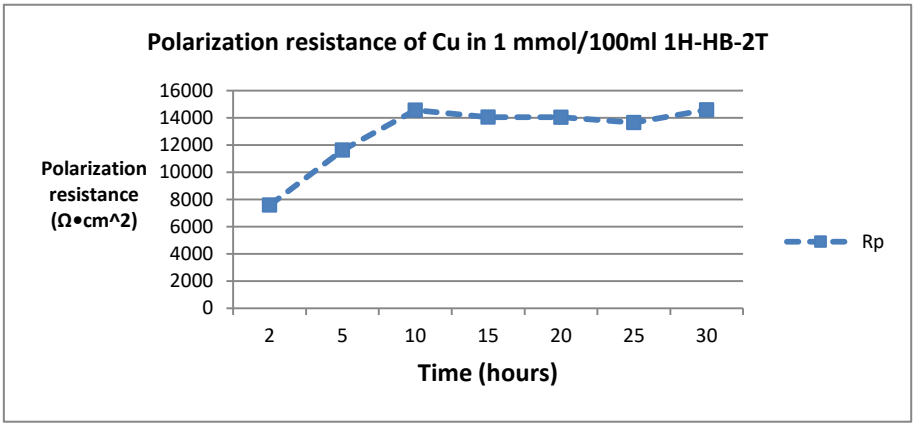

Figure E-3 The change of polarization resistance of Cu in 1 mmol/100ml 1H-HB-2T got from EIS

APPENDIX F

1 mmol/100ml 2-mercapto-1-methyl-benzimidazole (1H-HB-2T) on 50% Zn copper alloy film

Figure F-1 The equivalent circuit

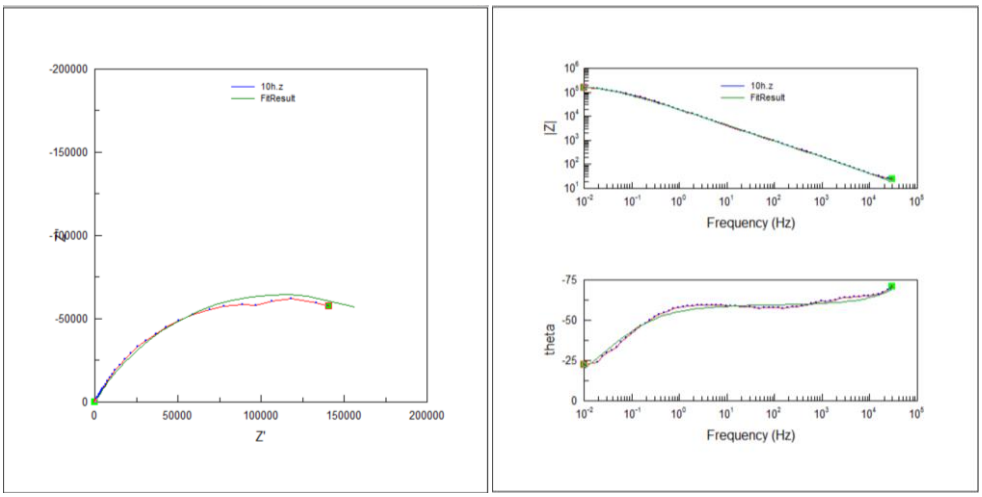

Figure F-2 The fitting plots

Table F-1 Impedance data after 2 hours of immersion

	Value	Error	Error%
R_s	-4.098	1.0632	25.944
C_{coat}-T	1.0431E-05	2.8647E-07	2.7463
C_{coat}-P	0.6901	0.0039421	0.57124
R_p	84707	2258.2	2.6659

Table F-2 Impedance data after 5 hours of immersion

	Value	Error	Error%
R_s	-3.445	0.43443	12.61
C_{coat}-T	1.3766E-05	1.339E-07	0.97269
C_{coat}-P	0.66999	0.0014365	0.21441
R_p	139680	2165.2	1.5501

Table F-3 Impedance data after 10 hours of immersion

	Value	Error	Error%
R_s	-3.927	0.49033	12.486
C_{coat}-T	1.4843E-05	1.5211E-07	1.0248
C_{coat}-P	0.66272	0.0015234	0.22987
R_p	224830	6112.3	2.7186

Table F-4 Impedance data after 15 hours of immersion

	Value	Error	Error%
R_s	-1.691	0.69738	41.241
C_{coat}-T	1.7319E-05	2.6648E-07	1.5387
C_{coat}-P	0.65941	0.002292	0.34758
R_p	181070	6360.6	3.5128

Table F-5 Impedance data after 20 hours of immersion

	Value	Error	Error%
R_s	-2.344	0.75307	32.128
C_{coat}-T	1.9137E-05	3.3529E-07	1.7521
C_{coat}-P	0.65475	0.0026001	0.29711
R_p	174630	7343.8	4.2053

Table F-6 Impedance data after 25 hours of immersion

	Value	Error	Error%
R_s	-4.203	2.7067	64.399
C_{coat}-T	2.0015E-05	1.4508E-06	7.2486
C_{coat}-P	0.65616	0.010476	1.5966
R_p	126520	16687	13.189

Table F-7 Impedance data after 30 hours of immersion

	Value	Error	Error%
R_s	-4.402	0.78163	17.756
C_{coat}-T	2.2922E-05	4.5211E-07	1.9724
C_{coat}-P	0.6432	0.0029055	0.45173
R_p	155040	7788.7	5.0237

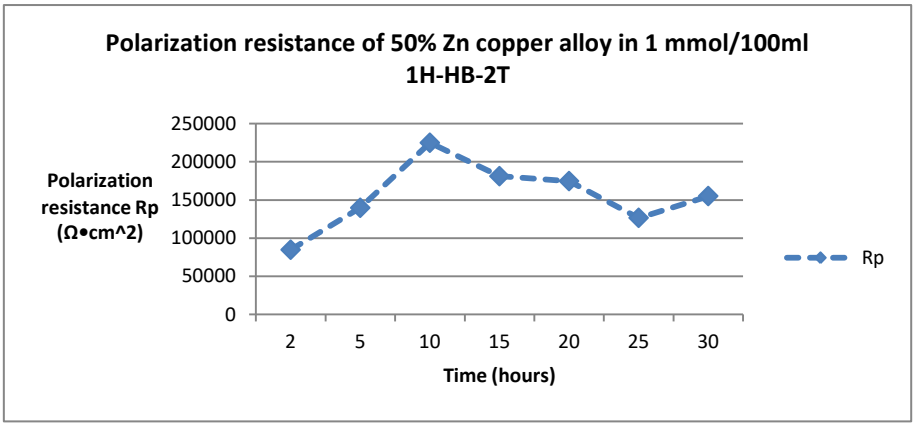

Figure F-3 The change of polarization resistance of 50% Zn copper alloy in 1 mmol/100ml 1H-HB-2T got from EIS

APPENDIX G

1 mmol/100ml 2-mercapto-1-methyl-benzimidazole (1H-HB-2T) on pure Zn film

Figure G-1 The equivalent circuit

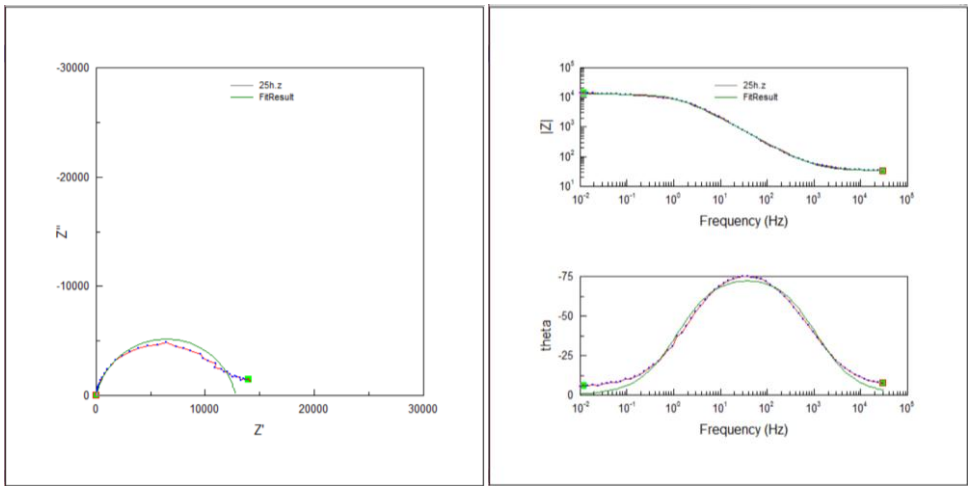

Figure G-2 The fitting plots

Table G-1 Impedance data after 2 hours of immersion

	Value	Error	Error%
R_s	16.74	1.33316	7.9546
C_{coat}-T	2.7688E-06	2.9443E-07	10.634
C_{coat}-P	0.84044	0.011869	1.4122
R_p	1594	26.963	1.6915

Table G-2 Impedance data after 5 hours of immersion

	Value	Error	Error%
R_s	7.6031E-05	4.3325	5.6983E06
C_{coat}-T	2.6345E-05	2.8535E-06	10.831
C_{coat}-P	0.57845	0.014212	2.4569
R_p	11053	595.1	5.3841

Table G-3 Impedance data after 10 hours of immersion

	Value	Error	Error%
R_s	17.96	3.0478	16.97
C_{coat}-T	4.0501E-05	2.1921E-06	5.4125
C_{coat}-P	0.5597	0.0078034	1.3942
R_p	17115	847.74	4.9532

Table G-4 Impedance data after 15 hours of immersion

	Value	Error	Error%
R_s	46.74	1.9612	4.196
C_{coat}-T	2.4261E-05	9.9442E-07	4.0988
C_{coat}-P	0.73386	0.0073054	0.99548
R_p	26159	938.84	3.589

Table G-5 Impedance data after 20 hours of immersion

	Value	Error	Error%
R_s	40.26	0.9292	2.308
C_{coat}-T	1.7968E-05	5.1576E-07	2.8704
C_{coat}-P	0.81605	0.0051198	0.62739
R_p	20722	407.95	1.9687

Table G-6 Impedance data after 25 hours of immersion

	Value	Error	Error%
R_s	33.92	0.47998	1.415
C_{coat}-T	1.3581E-05	3.0105E-07	2.2167
C_{coat}-P	0.86731	0.0037855	0.43646
R_p	12769	142.58	1.1166

Table G-7 Impedance data after 30 hours of immersion

	Value	Error	Error%
R_s	30.25	0.53209	1.759
C_{coat}-T	9.3427E-06	2.8539E-07	3.0547
C_{coat}-P	0.89903	0.0049532	0.55095
R_p	11435	148.75	1.3008

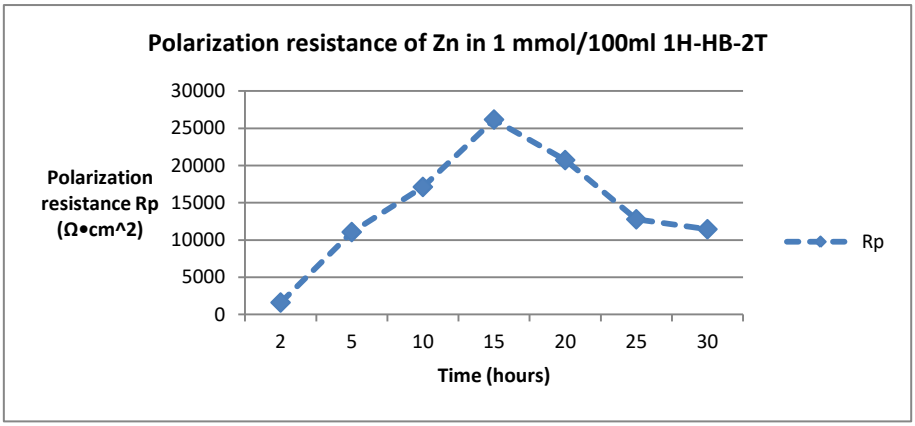

Figure G-3 The change of polarization resistance of Zn in 1 mmol/100ml 1H-HB-2T got from EIS

REFERENCES

[1]L.Nunez, E.Reguera, F.Corvo, et al. “Corrosion of copper in seawater and its aerosols in a tropical island”, *Corrosion Science*, Vol. 47, Issue 2, 2005, pp.461-484

[2]K.A.Nageh, A.N.Ahmed, A.A. Elsayed. “A review of the effects of benzotriazole on the corrosion of copper and copper alloys in clean and polluted environments”, *Journal of Applied Electrochemistry*, Vol. 39, Issue 7, 2009, pp.961-969

[3]H.Gerengi, M.Mielniczek, C.Gece, et al. “Experimental and quantum chemical evaluation of 8-hydroxyquinoline as a corrosion inhibitor for copper in 0.1 M HCl”, *Industrial and Engineering Chemistry Research.*, Vol.55, Issue 36, 2016, pp.9614-9624

[4]S.Hosseinpour, M.Forslund, C.Magnus Johnson, et al. “Atmospheric corrosion of Cu, Zn and Cu-Zn alloys protected by self-assembled monolayers of alkanethiols”, *Surface Science*, Vol.648, 2016, pp. 170-176

[5] http://chemistry.about.com/od/alloys/f/What-Is-Brass.htm

[6] https://en.wikipedia.org/wiki/Brass

[7]B.R.Milan, M.A.Milan. “Inhibition of brass corrosion by 2-Mercapto-1-methylimidazole in weakly alkaline solution”, *Journal of Materials Engineering and Performance*, Vol.25, Issue 3, 2016, pp.921-937

[8]H.Fan, S.Li, Z.Zhao, et al. “Inhibition of brass corrosion in sodium chloride solutions by self-assembled silane films”, *Corrosion Science*, Vol.53, Issue 12, 2011, pp.4273-4281

[9]A.Rochdi, O.Kassou, N.Dkhireche, et al. “Inhibitive properties of 2,5-bis(n-methylphenyl)-1,3,4-oxadiazole and biocide on corrosion, biocorrosion and scaling controls of brass in simulated cooling water”, *Corrosion Science*, Vol.80, 2014, pp.442-452

[10]R.X.Joseph. “Inhibition effect of Thiadiazole piperidine and oxadiazole derivatives on brass corrosion in natural seawater”, PhD Thesis, University of Anna, India, 2013

[11]P.B. Raja, M.G. Sethuraman. “Natural products as corrosion inhibitor for metals in corrosive media”, *Materials Letters*, Vol.62, Issue 1, 2008, pp. 113-116

[12]T.A.Soylev, M.G.Richardson. “Corrosion inhibitors for steel in concrete:

State-of-the-art report", *Construction and Building Materials*, Vol.22, Issue 4, 2008, pp.609-622

[13] http://www.substech.com/dokuwiki/doku.php?id=corrosion_inhibitors

[14]B.Hmmouti, A.Dafali, R.Touzani, et al. "Inhibition of copper corrosion by bipyrazole compound in aerated 3% NaCl", *Journal of Saudi Chemical Society*, Vol.16, Issue 4, 2012, pp.413-418

[15]A.S.Fouda, S.M.Rashwan, M.Kamel, et al. "Unused meropenem drug as corrosion inhibitor for copper in acidic medium: experimental and theoretical studies", *International Journal of Electrochemical Science*, Vol.11, 2016, pp.9745-9761

[16]J.Aljourani, K.Raeissi, M.A.Golozar. "Benzimidazole and its derivatives as corrosion inhibitors for mild steel in 1 M HCl solution", *Corrosion Science*, Vol.51, Issue 8, 2009, pp.1836-1843

[17]X.J.Raj, N.Rajendran. "Effect of some oxadiazole derivatives on the corrosion inhibition of brass innatural seawater", *Journal of Materials Engineering and Performance*, Vol.21, Issue 7, 2012, pp.1363-1373

[18]https://www.corrosionpedia.com/definition/834/open-circuit-potential-ocp

[19]H.F.Okorn-Schmidt, C.D'Emic, R.Murphy. "Characterization of DI water/O3 oxidation of Si (100) and Si (111) surfaces by OCP measurements", *Solid State Phenomena*, Vols.76-77, 2001, pp.161-164

[20]T.Lim, K.Park, M.Kim, et al. "Real-time observation of Cu electroless deposition using OCP measurement assisted by QCM", *Journal of the Electrochemical Society*, Vol.159, Issue 12, 2012, pp.D724-D729

[21]J.P.Wilburn, M.Ciobanu, D.A.Lowy. "Characterization of acrylic hydrogels by open circuit potential monitoring", *Journal of Applied Electrochemistry*, Vol.34, Issue 7, 2004, pp.729-734

[22]R.Solmaz. "Investigation of adsorption and corrosion inhibition of mild steel in hydrochloric acid solution by 5-(4-Dimethylaminobenzylidene) rhodanine", *Corrosion Science*, Vol.79, 2014, pp.169-176

[23]C.Andrade, C.Alonso, J.Gulikers, et al. "Test methods for on-site corrosion rate measurement of steel reinforcement in concrete by means of the polarization resistance method", *Materials and Structures*, Vol.37, 2004, pp.623-643

[24]S.K.Shukla, A.K.Singh, M.A.Quraishi. "Corrosion inhibition and adsorption

properties of N-Phenylhydrazine-1,2-Dicarbothioamide on mild steel in hydrochloric acid", *International Journal of Electrochemical Science*, Vol.6, Issue 11, 2011, pp.5779-5791

[25]D.Loveday, P.Peterson, B.Rodgers. "Evaluation of organic coatings with Electrochemical Impedance Spectroscopy, Part 1: fundamental of Electrochemical Impedance Spectroscopy", *JCT Coatings Tech*, 2004, pp.46-52

[26]G.Bierwagen, D.Tallman, J.Li, et al. "EIS studies of coated metals in accelerated exposure", *Progress in Organic Coatings*, Vol.46, Issue 2, 2003, pp.148-157

[27]http://www.metrohm-autolab.com/download/Applicationnotes/Autolab_Application_Note_EIS03.pdf

[28] I.Milosev, N.Kovacevic, J.Kovac, et al. "The roles of mercapto, benzene and methyl groups in the corrosion inhibition of imidazoles on copper: I. Experimental characterization", *Corrosion Science*, Vol.98, 2015, pp.107-118

[29]P.Zhang, Q.Zhu, Q.Su, et al. "Corrosion behavior of T2 copper in 3.5% sodium chloride solution treated by rotating electromagnetic field", *Transactions of Nonferrous Metals Society of China*, Vol.26, Issue 5, 2016, pp.1439-1446

[30] http://www.shimadzu.com/an/ftir/support/faq/4.html

[31]M.R.Ahamed, S.F.Narren and A.S.Sadiq. "Synthesis of 2-mercaptobenzimidazole and some of its derivatives", *Journal of Al-Nahrain University*, Vol.16, Issue 2, 2013, pp.77-83

[32]M.G.Hosseini, T.Shanrabi and R.J.Nichols. "Characterization of mercaptobenzimidazole adsorption on an Au(111) electrode", *Iranian Journal of Science and Technology*, Vol.29, Issue A1, 2005, pp.49-63

[33]A.Zarrouk, B.Hammouti, A.Dafali, et al. "A theoretical study on the inhibition efficiencies of some quinoxalines as corrosion inhibitors of copper in nitric acid", *Journal of Saudi Chemical Society*, Vol.18, Issue 5, 2014, pp.450-455

[34]M.Mouanga, P.Bercot, J.Y.Rauch. "Comparison of corrosion behavior of zinc in NaCl and in NaOH solutions. Part 1: Corrosion layer characterization", *Corrosion Science*, Vol.52, Issue 12, 2010, pp. 3984-3992

Acknowledgements

I would like to express my most sincere gratitude to my supervisors, Dr. J.M.C. Mol and Dr. P. Taheri, for their invaluable knowledge and advice as well as their guidance, support and understanding.

Special thanks are directed to everyone in corrosion groups for their valuable advice and friendly help during my thesis. In particular, I would also like to extend my gratitude to Agnieszka for helping me a lot on lab/ instruments issues.

I would also like to take this opportunity to thank all my tutors as well as all my classmates during my two-year Master period.

Last but not least, I would like to thank my family for their patience, encouragement and support. Without you, I will not have the opportunity to come here for my Master study.

Because of you all, I spent the most unforgetable two years in the Netherlands, in TU Delft, thank you very much.